THESIS

MEASUREMENT OF LOW-ALTITUDE AEROSOL LAYERS SURROUNDING CONVECTIVE COLD POOL PASSAGE OBSERVED BY UNCREWED AIRCRAFT

Submitted by

Brian Heffernan

Department of Atmospheric Science

In partial fulfillment of the requirements

For the Degree of Master of Science

Colorado State University

Fort Collins, Colorado

Summer 2024

Master's Committee:

Advisor: Sonia Kreidenweis
Co-Advisor: Russell Perkins

Jeffrey Pierce
Shantanu Jathar

ABSTRACT

MEASUREMENT OF LOW-ALTITUDE AEROSOL LAYERS SURROUNDING CONVECTIVE COLD POOL PASSAGE OBSERVED BY UNCREWED AIRCRAFT

Convectively generated cold pools can have myriad impacts on local aerosol concentrations. Passage of cold pools may loft dust, pollen or other aerosols from the surface, and precipitation and humidity changes accompanying cold pools also impact local aerosols in several ways. The vertical profile of aerosols can have important effects on meteorology, however, the effects of cold pools on the vertical distribution of aerosol are largely unstudied. During the BioAerosol and Convective Storms (BACS) field campaigns in the Colorado plains in spring of 2022 and 2023, Uncrewed Aircraft (UA) were utilized to observe the vertical profile of aerosol, and how this vertical profile may be affected by the passage of cold pools. UAs with mounted aerosol and meteorological instrument packages were deployed in a vertical column to profile different atmospheric variables. Flights were conducted before, during, and after the passage of cold pools, and UA data were contextualized using radiosonde measurements and surface-based aerosol and meteorological instruments.

A discussion of the challenges of UA-mounted aerosol sampling is presented. Validation experiments were conducted to assess the reliability of UA-mounted Optical Particle Counters (OPCs), and analyzed to show that UA-mounted OPCs can provide reliable data under certain circumstances. Two primary issues are discussed in detail: sensor drift and suppressed OPC sampling flow. A calibration procedure was developed and utilized to address the issue of sensor drift, while suppressed OPC sample flow was addressed by removing all data below a determined critical threshold flow rate. These methodologies lead to the creation of a robust data product for the measurement of aerosol vertical profiles using UA-mounted OPCs.

Using these OPC data, an analysis of the vertical profiles observed during the BACS campaign

is provided, up to 350m above the surface. We find that a common feature of a post cold pool environment is a layer of enhanced submicron aerosol concentration measured 120m above the surface. This feature and its evolution are examined in detail for several case studies, and different possible explanations are presented. Potential causes of this observed feature include pollen-rupture, low temperature inversions trapping aerosol in a low stable layer of elevated aerosol concentration, and emission and/or deposition of aerosols, but these explanations each appear to be insufficient. This feature appears to be caused by the dynamics of the cold pool, which can entrain and redistribute airmasses from different levels of the atmosphere.

ACKNOWLEDGEMENTS

Support for this work was provided by the National Science Foundation Division of Atmospheric and Geospace Sciences through grant AGS-2105938. The National Ecological Observatory Network is a program sponsored by the National Science Foundation and operated under cooperative agreement by Battelle. This material is based in part upon work supported by the National Science Foundation through the NEON Program. Data collected/used in this research were obtained through the NEON Assignable Assets program. We would like to acknowledge support for this project from the United States Department of Agriculture agency of Agricultural Research Services by providing site access at the Central Plains Experimental Range. Special thanks to Amy Bibbey and Troy Bauder and other staff at the Colorado Agricultural Experiment Station for help in supporting and scheduling facilities at the Semi-arid Grasslands Research Center.

I would also like to extend my deepest gratitude to those who have supported and guided me through my academic journey at Colorado State University. First I would like to thank my advisor, Snia Kreidenweis and Co-advisor, Russel Perkins, as well as every other member of the Kreidenweis group at CSU for creating a great scientific environment. I would also like to thank all my professors and classmates at CSU who helped me to obtain the education necessary to complete this project. FInally I would like to thank all the support staff at CSU for making everything possible.

TABLE OF CONTENTS

CHAPTER 1: INTRODUCTION

1.1 Cloud Condensation Nuclei and Ice Nucleating Particles

Aerosols, liquid or solid particles suspended in Earth's atmosphere, play crucial roles in global climate and weather. A major pathway through which aerosols affect weather and climate is by acting as cloud condensation nuclei (CCN). CCN act as a site at which cloud droplets form and grow after local relative humidities reach supersaturation, with required supersaturation for activation depending on particle size and hygroscopicity (Petters and Kreidenweis, 2007). Additionally, some atmospheric particles can act as ice nucleating particles (INP), which allow for the formation of ice crystals at temperatures warmer than the -38°C necessary for homogeneous nucleation (Kanji et al. 2017).

These two types of atmospheric aerosol exhibit significant influence on global climate as well as local meteorology. However, their effects are myriad and multifaceted. In addition to being necessary for the formation of clouds, CCN and INP have important impacts on cloud properties including precipitation development, and influence radiative transfer and cloud electrification (Kanji 2017, Rosenfeld 2014). Characterization of these cloud-relevant aerosols are most important at the altitudes where cloud formation occurs, but the majority of measurements occur at the ground for logistical reasons. A robust understanding of aerosol vertical gradients will help us understand how ground-based measurements can be applied to cloud-level processes.

Among the most abundant atmospheric aerosol is mineral dust. Mineral dust enters Earth's atmosphere most commonly as wind blows against the erodible surface. Collisions between different sized particles at the surface lead to small (<20μm) particles ejecting from the surface into the atmosphere, where they can be suspended for weeks and travel thousands of kilometers under some circumstances (Kok 2012). The surface wind necessary to eject this dust can be caused by a myriad of meteorological phenomena, from large synoptic cyclones, to localized cold pools, which can loft dust

along their outer walls to form haboobs. After lofting, mineral dust forms an important source of CCN (Pringle et al. 2010) and INP (DeMott 2010) in Earth's atmosphere.

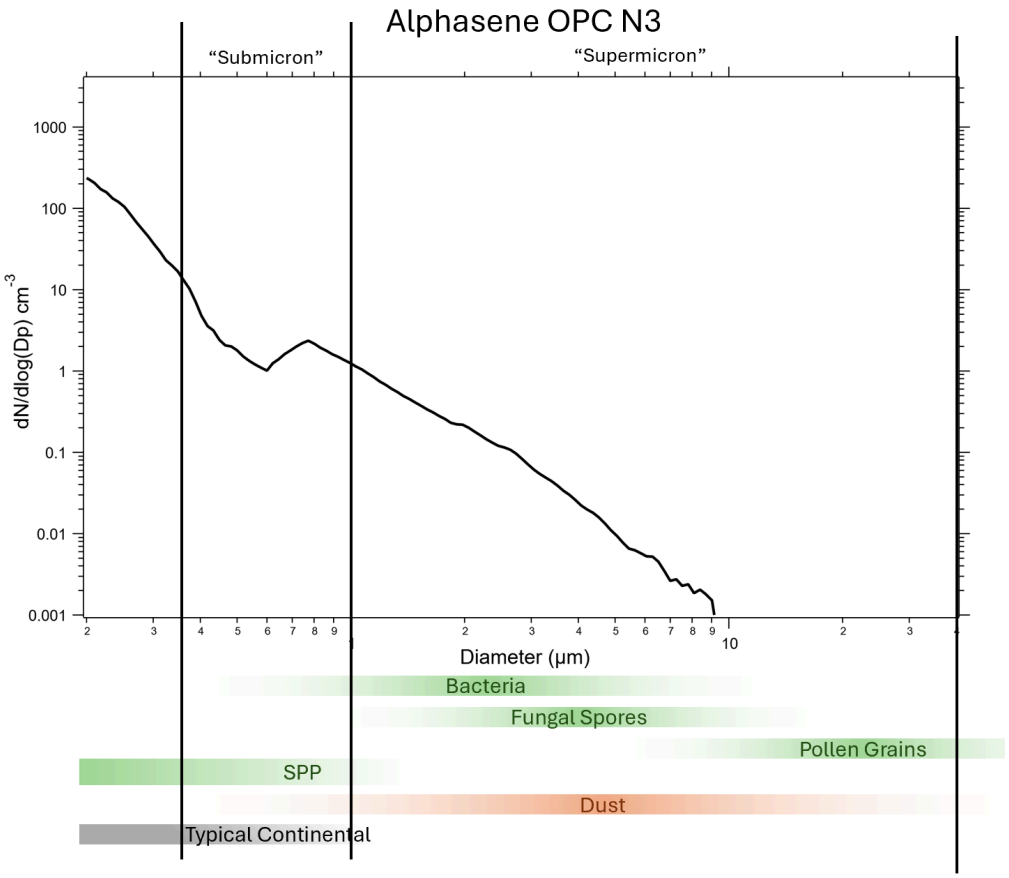

Figure 1.1: Size range of relevant aerosol types, as compared to a prototypical aerosol size distribution measured during the BACS field campaign, overlaid with the supermicron and submicron measurement categories used in this study, based on the measurement range of the drone-mounted optical particle counter used in this experiment. Green highlighted aerosol types are the main types of biological aerosols discussed in this work. Data adapted from (Després et al. 2012, Taylor et al. 2004, Seinfeld & Pandis 2016).

CCN are most effective (require lower supersaturation for activation) at larger particle diameters, and there is some evidence that IN activity also increases at larger particle diameters. DeMott et al. (2010) found that the concentration of INP was strongly associated with the number concentrations of particles

with diameters >0.5μm. This size range will include submicron particles such as SPP and smaller bacteria, as well as supermicron particles: larger bacteria, intact pollen grains, and fungal spores. Mineral dust, and therefore mixed bioaerosol, also may be either supermicron or submicron. Other continental aerosol sources, such as low volatility photochemical products like sulfate and nitrate species and organic aerosol will also appear in this size range to some extent, but are generally not believed to be an important source of immersion-mode INP. Biomass burning aerosol can be a significant source of INP (Barry et al. 2021). As will be noted, periods of heavy smoke influence were observed during one of our campaigns, and smoke may be a significant INP source during those periods.

1.2 Bioaerosols

In addition to mineral dust, bioaerosols are a subset of aerosols which may have important impacts on meteorology and climate. Bioaerosols are defined here as primary aerosols of biogenic origin. Examples of bioaerosols include fungal spores, bacteria, and pollen, with approximate size ranges shown in Figure 1.1. These bioaerosols have been shown to be an important source of both CCN (Steiner 2015) and INP (e.g., Conen et al. 2011, Pummer et al. 2015). Biological material may also adsorb to the surface of or otherwise mix with non-biological aerosol to create a mixed particle; O'Sullivan et al. (2016) found that ice nucleating fungal proteins preferentially bind to a common soil mineral. Internally mixed particles tend to have the same ice-nucleating properties as their most ice-active constituent (Augustin-Bauditz et al. 2016, Conen et al. 2011), so these mixed bioaerosol may be an important source of INP. For the purposes of this paper, these mixed particles will also be considered bioaerosol.

The emission and deposition of bioaerosol has also been shown to be highly dependent on meteorological conditions. Huffman et al. (2013) found that the concentration of airborne bioaerosol, as measured at the surface, increased after rainfall and swiftly decayed afterwards. Under high relative humidity conditions, pollen grains can rupture into many, smaller sub-pollen particles (SPPs). For instance, Taylor et al. (2004) in a laboratory study measured the emission of SPPs ranging from 30 nm - 4 μm upon the rupture of birch pollen grains, which measured approximately 20 μm in diameter while

intact. Observational studies have shown that accompanying precipitation, there is a significant increase in SPPs (Rathnayake et al.2016, Hughes et al. 2020), which may act as CCN or INP in the atmosphere. A recent modeling study has suggested that pollen rupture may increase cloud ice and water by up to 50% and that SPP have a larger impact on cloud processes than intact pollen grains (Zhang et al. 2024).

1.3 Aerosol Measurement

As mentioned previously, CCN and INP only fulfill their function when at high enough altitudes to form clouds, so CCN and INP measurements at the surface may not be sufficient to understand their meteorological impacts. CCN and INP from mineral dust and bioaerosol are obviously generated at the surface and, as the sun heats the surface, convectively driven turbulence mixes them throughout a shallow layer of well mixed air, known as the mixed layer (ML) (Stull, 1988). Aerosol composition is often assumed to be constant, or nearly constant within the ML due to this mixing (Li et al. 2017), and it is often assumed that aerosol number concentrations can be approximated by a smooth, monotonic exponential decay from the surface concentration, assuming a characteristics scale height (Jaenicke 1993). Experimental data often support these assumptions. Delle Monache et al. (2004) report that across many varied meteorological conditions, both extensive and intensive properties of atmospheric aerosol within the boundary layer are highly correlated with surface measurements, suggesting that aloft measurements can be derived from surface measurements alone in some cases. However, cases have also been observed in which aerosol concentrations do not relate monotonically with height. Aerosol concentrations can be significantly higher aloft than at the surface, for example, stratified layers with elevated aerosol concentration are commonly found directly below a low-altitude temperature inversion. Liu et al. (2020) noted elevated PM 2.5 near the top of the boundary layer during a haze event in Nanjing. Creamean et al. (2021) found that in the remote arctic “spikes” of elevated aerosol concentration were frequently associated with temperature inversions and occurred at similar heights.

One major inhibition to understanding aerosol vertical profiles, and the conditions that give rise to anomalous gradients, is the lack of experimental in-situ collections of aerosol vertical profiles. Much data

on atmospheric aerosol comes from ground-based measurements, such as the Aerosol Robotic Network (AERONET), a network of sun photometers measuring aerosol optical depth (AOD). AERONET reports column-integrated values, but does not offer vertical profiling (Holben et al. 1998). Methods of estimating aerosol vertical profiles often depend on certain models or assumptions. For example, AOD measurements may be converted into aerosol vertical profiles based on certain assumptions about the general shape of the profile, such as assuming a well-mixed lower atmosphere. These assumptions have been shown to introduce biases into optical thickness measurements in some cases (Rozwadowska 2007). Additionally, many remote-sensing observational instruments,such as the Cloud-Aerosol Lidar and Infrared Pathfinder Satellite Observation (CALIPSO), do not provide reliable data for the lowest few hundred meters of the atmosphere due to surface effects (Kim et al. 2017). This surface region is critical to relating ground-based measurements to those aloft.

In addition to remote sensing, several different methods of in-situ measurement are also utilized for obtaining aerosol vertical profiles. One common method is the use of meteorological observation towers (e.g., Sun et al. 2020, Lei et al. 2021), which come with the obvious drawbacks of requiring significant infrastructure and having limited height. Due to this, at present meteorological observation towers tall enough to measure aerosol vertical profiles are few and far between. The National Ecological Observatory Network (NEON) is a network of observation towers ranging from 8-74m in height, spread throughout the United States, though these are primarily used to facilitate flux measurements rather than gather vertical profiles. Another technique is measurement using traditional, piloted aircraft flights, (e.g., Andrews et al. 2007; Liu et al., 2009) which are relatively expensive and, for reasons of safety and practicality, typically do not measure in the lower few hundred meters of the atmosphere. Most recently, tethered balloons have proven a useful platform from which to measure aerosol vertical profiles (e.g., Greenberg and Turnipseed 2009, Creamean et al. 2018). Ascending balloon measurements have also been used to measure aerosol profiles into the stratosphere (Todt et al. 2023), though the recovery of instrument packages after introduces significant cost and difficulty to this kind of experiment

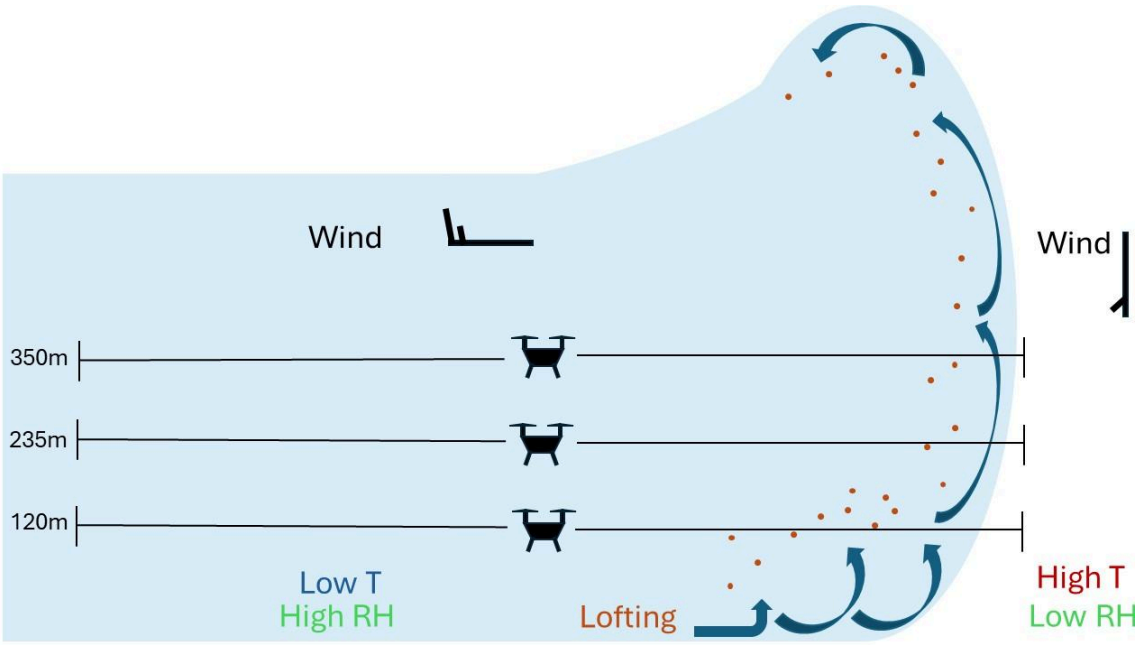

Figure 1.2: Schematic of typical cold pool passage and drone flights during BACS field campaign

In addition to these approaches, uncrewed aircraft (UAs) have become widely utilized due to their relative cost-effectiveness, ease of operation, and versatility in deployment across various altitudes and geographic locations. For example, Altstädter et al. (2015) utilized a condensation particle counter (CPC) mounted to a UA to measure ultrafine particles in order to study new particle formation (NPF), and Kwak et al. (2020) used a UA-mounted micro-aethalometer in tandem with a observation tower to monitor airborne black carbon concentrations in rural South Korea. A further discussion of the nuances of UA-based measurement is included in the methods section of this paper. While UA-based methods have been successfully utilized to measure aerosol vertical profiles in the past, this study is, to the best of the authors' knowledge, the first to use these techniques to study the effects of cold pool passage on aerosol vertical profiles.

1.4 Impacts of Meteorology on Aerosol

Cold pools are outflows of evaporatively-cooled air formed beneath a precipitating cloud, particularly around thunderstorms. As precipitation falls out of the cloud outside of the main updraft region, evaporative cooling causes density changes in the air it is falling through, in turn causing that air to sink toward the surface and entraining free tropospheric into the "head" of cool air that spreads along the surface (Goff 1976). This air likely brings along aerosol from the free troposphere with it. In addition to potential changes in aerosol, cold pools have many important impacts on meteorology, via maintaining (Rio et al. 2009) and initiating (Droegemeier and Wilhelmson 1985) other convective storms. The strong wind front of a cold pool may loft mineral dust from the surface (Kok et al. 2012, Saleeby et al. 2019). Besides surface lofting, cold pool dynamics may have significant impacts on vertical aerosol profiles. As Seigel and van den Heever (2012) show in a modeling study, turbulent mixing caused by cold pool downdrafts can lead dusty air at the cold pool head to be forced towards the back of the cold pool under certain conditions, resulting in non-monotonic changes in aerosol concentrations with height.

In addition to the dynamical impact of cold pools on aerosol populations, convective storms and cold pools also may increase the prevalence of bioaerosols. The precipitation and high RH brought by convective storms can lead to the release of many different types of bioaerosol, including fungal spores, pollen, and bacteria (Fröhlich-Nowoisky et al. 2016). Besides direct emission changes, convective storms and cold pools can cause an increase in SPP via increasing RH, causing the pollen to rupture (Hughes et al. 2020). These particles may then, in turn, be lofted into the atmosphere and impact the meteorological development of subsequent or even parent storms through changes in cloud-relevant INP and CCN abundances.

1.5 The BACS Campaign

The BioAerosols and Convective Storms (BACS) field campaign consisted of two phases, taking place during May and June in 2022 and 2023, at and near the Central Plains Experimental Range (CPER), near Nunn, Colorado. This location and season were selected to maximize opportunities to study convective storms and cold pools, which form readily over the plains in the springtime. The nearby National Ecological Observatory Network (NEON) flux tower allowed for measurements to be performed

from above the surface, discussed further below. The abundance of pollen from local grasses and trees, as well as fungal spore concentrations also made CPER an ideal location for the study of the interactions between cold pools and bioaerosol.

1.6 Thesis Outline and Objectives

This project was undertaken to explore how aerosol vertical profiles, in a rural setting, respond to storm dynamics, and in particular to the passage of cold pools. This topic is the subject of the BACS campaign, along with the design of the measurement strategy for vertical profiles of sub- and supermicron particles. The results from the two springtime BACS field campaigns are presented in Chapter 3, ideas for and overall findings are summarized in Chapter 4, and ideas for future work are presented in Chapter 5

CHAPTER 2: METHODS

2.1 Experimental Design and Procedure

Throughout the course of the two campaign periods of BACS, days in which weather forecasts were particularly favorable to the formation of convective storms, and therefore cold pools, were selected to be intensive operation periods (IOPs) by the BACS forecasting team. During IOPs UA flights were organized to measure aerosol vertical profiles. In an ideal case, each IOP began with a pre-convective flight to establish environmental conditions. Afterwards, flights would be conducted both before and after the passage of cold pools to study their effect on aerosol profiles. As cold pools are associated with convective storms and precipitation, inclement weather sometimes caused one or more of these flights not to occur. During a given flight, the three UAs were flown to their predetermined altitudes of 120, 235, and 350m. These heights were selected to evenly distribute measurements throughout the boundary layer, up to the maximum altitude allowed by the Federal Aviation Administration waiver granted to our group (365 m). A few flights at different pre-set altitudes were performed during this campaign, but are not discussed in this paper. For the passage of a typical BACS cold pool, this meant that all three UAs were within the cold pool. A schematic of this arrangement is presented in Figure 1.2 The UAs were organized in a column, flown at equal latitudinal and longitudinal coordinates, to the extent that was reasonably possible. The UAs remained in column formation until either battery or weather conditions dictated they return to the surface, generally for flight periods of 10-20 minutes.

2.2 UA Instrumentation

While a large ensemble of aerosol instrumentation was utilized during this experiment, this paper offers particular focus on optical particle counter (OPC) measurements. For the duration of the two phases of the campaign, both surface and drone-mounted OPC data were collected. The precise arrangement of OPCs differs slightly between BACS-I and BACS-II, though for every experiment there was an attempt to

have OPC measurements at the surface, 120m, and 350m levels, and many flights also have OPC measurements at the 235m level.

Individual OPCs were mounted to DJI Matrice 600 drones and flown throughout the atmospheric boundary layer. Five Alphasense OPC N3s were utilized in this experiment for both UA-mounted and surface-based measurements. According to the manufacturer, the N3 measures particles nominally from 0.35-40μm in diameter and counts ~100% of particles greater than its lower limit of 350 nm in diameter (Technical Specifications OPC-N3 Particle Monitor 2019) and. This size range covers several important types of aerosol expected in the BACS study, including pollen, SPP, mineral dust, and others, as shown in Figure 1.1. The Alphasense OPC detects, counts and sizes particles by passing a sampled air stream through the beam of aa laser of nominal wavelength of 658 nm, t and an elliptical mirror to focus the scattered light from a range of angles onto its photodiode detector. Particles are then sorted into 24 size bins ranging from 330 nm - 40 μm in diameter. The instruments are calibrated by the manufacturer to polystyrene latex spheres (PSL) with a refractive index of ~1.6 and this calibration was not changed for these experiments. Calibration was validated by comparing OPC measurements to those generated by a merged size distribution generated from a combination of instruments, discussed in more detail below. For the BACS study, these OPCs were equipped with Arduino Teensy 4.1 development boards in order to obtain and store timestamped data. This modification and the software utilized by it were developed by our research group.

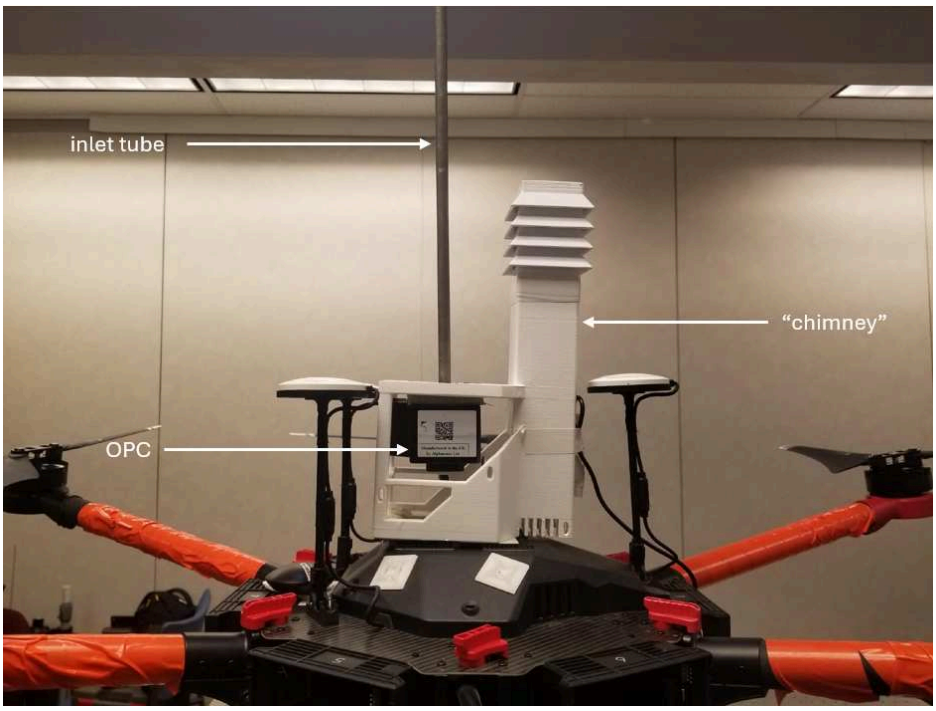

Figure 2.1: Photograph of UA-mounted instrument package

Alphasense OPCs generate flow via a small, 5V fan and sample at a nominal rate of 280 mL min^{-1}. The sensors report a measured flow rate, calculated from particle time-of-flight using a proprietary method, and these flow rate data were used in this study to calculate total particle number concentrations. Concentrations were calculated using the reported raw counts, flow rate, and sampling period.

$$Number\ Concentration\ (mL^{-1}) = raw\ counts * \frac{1}{Sampling\ Period\ (s)} * \frac{1}{flow\ (\frac{mL}{s})}$$

Equation 2.1: Conversion of OPC measured raw counts to number concentration

Drone-mounted OPC sampling was designed by the BACS team to ensure that sampled air was representative of ambient air. Because turbulent mixing caused by propellers extends further below a

multirotor drone than above (Crazzolara et al. 2019.), OPCs were mounted on the top of the drone body (Figure 2.1) and air was sampled via a one foot long vertical inlet tube of inner diameter 0.305 inches that extended above the rotors. This distance of clearance above the rotors is supported by the literature as well as experiments done using this orientation, described below. The OPC was mounted in a 3D printed "chimney", built primarily to aspirate a meteorological state variables sensor, as described in (Freeman et al. 2024).

2.3 UA Measurement Validation

UA measurement literature, both based on modeling of flow (Haas et al. 2014) and experimental testing (Crazzolara et al. 2019) demonstrate that the impact of UAV rotors on the surrounding air pressure and velocity is more pronounced below the UAV than above it, and are small in the center of all rotors, supporting our decision to mount the OPC above the UA and close to its center. However, as others (Liu et al. 2021) have noted, high wind speeds can have a significant impact on the accuracy of drone-based particle measurements. The Alphasense OPC uses a small (5V) fan to control sample flow into the instrument, which will be sensitive to pressure drop in the inlet. It reports flow using a proprietary time-of-flight calculation routine. For this reason we designed an experiment to test the potential effects of rotors on OPC air sampling, described below.

This intercomparison utilized an 8m tall NEON tower in Sterling, Colorado. One OPC was placed at the tower top and another mounted on a UA and flown at equal altitude nearby. Conditions on this day were very windy. Unfortunately an instrument outage prevented measurement of winds at the same altitude as the two OPCs, but the nearby weather station at Sterling Municipal airport measured sustained winds of 10-15 mph and gusts as high as 26 mph at the surface during this period (Iowa Environmental Mesonet, 2024). Likely because of these high winds, the reported OPC flow rates of both the drone-mounted and tower-mounted OPCs. dropped as low as 0.2 mL min^{-1}, less than 10% its nominal value (Figure 2.2), and caused the two OPCs to measure significantly different concentrations from one another, sometimes differing by as much as a factor of three.

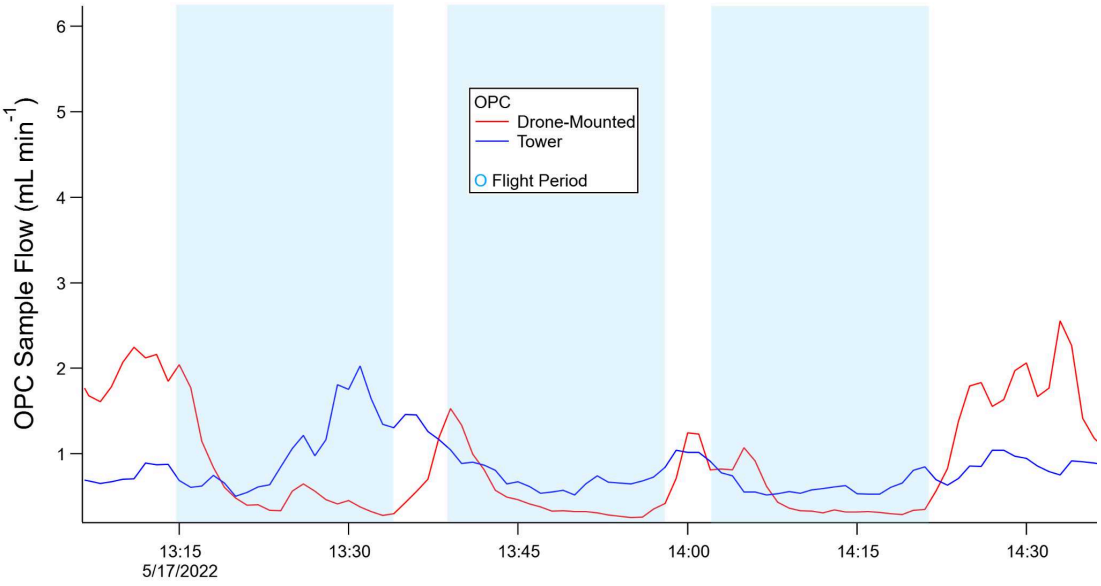

Figure 2.2: OPC flow rates reported during the Sterling Experiment on 5/17/2022. Blue highlighted regions represent flight periods.

In an attempt to study the effect of UA rotors on OPC measurement in a lower wind environment, we designed a second experiment. One OPC was mounted to a UA in the manner described above, while two other OPCs were mounted to a twenty foot tall pole, that was subsequently affixed to the ground, located at Christman Airfield in Fort Collins, CO. The tall pole was used to eliminate aerosol emissions due to propellor wash producing aerosol from the ground and convoluting the observations. The UA was then held stationary so that all OPCs were sampling air from an equal altitude at a horizontal offset of ~10 feet. The results of this experiment on measurement of both supermicron and submicron particle concentrations can be seen from the comparison of flight-averaged (Figure 2.3) and minute-averaged (Figure 2.4) data, and suggest that some component of the standard deviation calculated in the flight-averaged case is due to changes in aerosol concentrations over the flight window, and are an overestimation as a metric of the random error in the measurement.

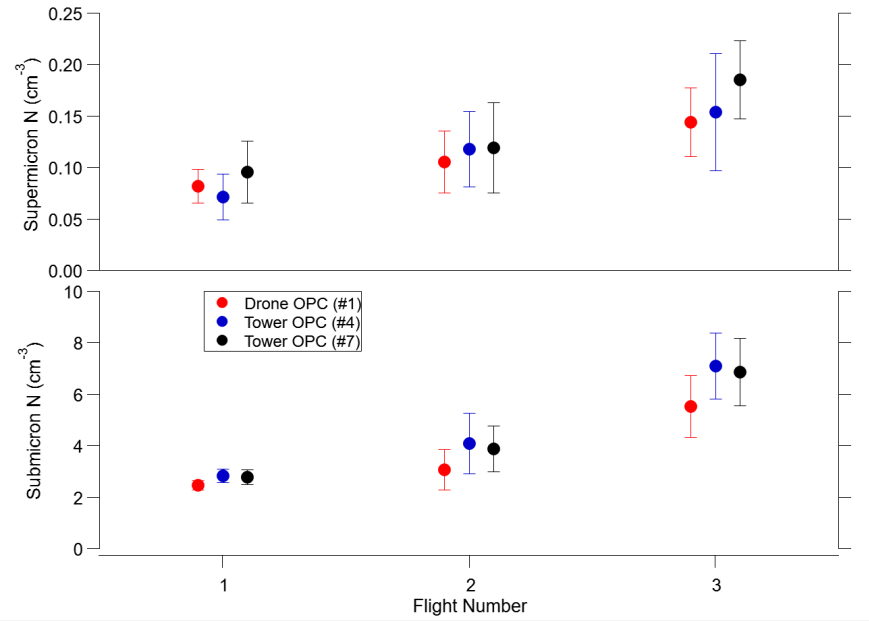

Figure 2.3: Flight-averaged aerosol concentrations as measured on both the drone-mounted and pole-mounted OPCs as measured during the Christman Airfield experiment

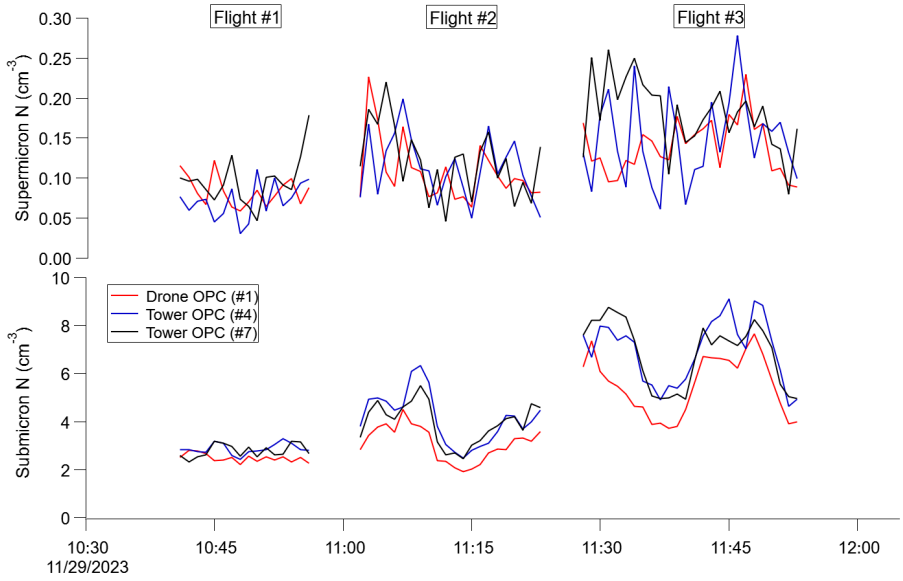

Figure 2.4: Minute-averaged aerosol concentrations as measured by the drone-mounted and pole-mounted OPCs during the Christman Airfield experiment

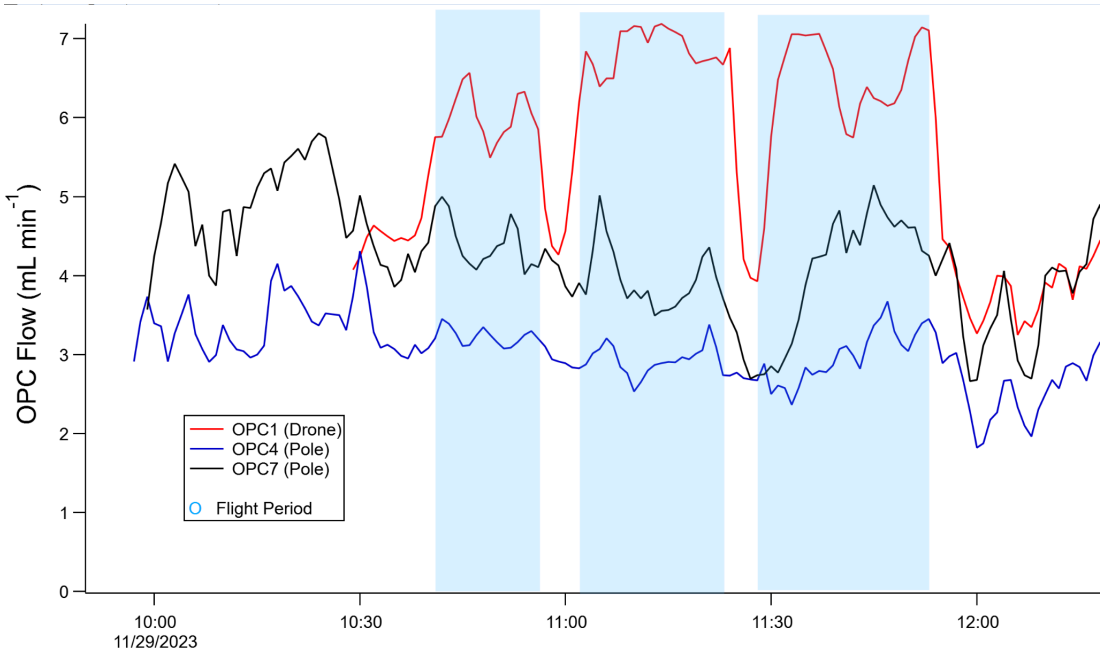

Figure 2.5: OPC flow rates as measured by UA- and Pole-mounted OPCs during the Christman Field experiment on 11/29/2023

At the low wind conditions present during this experiment the UA propellers may have impacted the OPC measured flow rate. However, the particle number concentrations as measured on the UA vs the tower were comparable. Across the three flights, in the supermicron channel, the UA mounted OPC (Figure 2.4, red) measured number concentrations closer in value to one pole-mounted OPC (blue) than the two pole-mounted OPCs did to one another. In the submicron channel, on the other hand, the UA mounted OPC measured ~20% lower than the pole-mounted OPCs across all three flights. The nature of the BACS campaign gives an opportunity to compare this result to other measurements of co-located OPCs. Often, for long periods in-between flights, the UAs were grounded and outdoors ~50ft away from the surface-mounted OPC. As Figure 2.6 shows, a ~20% difference is within the range of normally observed measurement differences for co-located OPCs, indicating that the airborne measurements were not drastically perturbed by the airflow of the UA. The observed difference between sensors on the ground was compensated for in our analysis, as described in section 2.5.

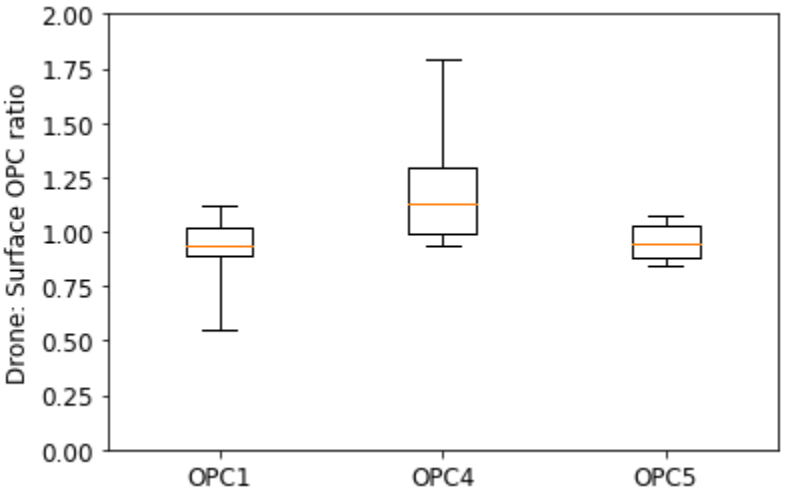

Figure 2.6: Submicron number concentration ratios for UA-mounted OPCs versus surface-mounted OPC during baseline periods of BACS-II

The UA instrument package utilized during the BACS campaigns did not include a drone mounted anemometer or any other method of reliably measuring wind speed from the drone. Due to this, and the fact that wind speeds can differ greatly between the surface and 350m aloft, the OPC-reported flow data were used to identify periods where wind speeds became too high for the OPCs to reliably measure. We determined that all OPC data which had reported flow rates below 0.5mL/min would be discarded, and are not analyzed here. This threshold was chosen to be conservative based on the results of the above experiments.

2.4 Surface Instrumentation

For several periods of the campaign, ground-based OPC measurements typically used for comparison with airborne measurements are missing, generally due to instrument errors. In these cases the OPC measurements were compared to data from a collection of other aerosol instrumentation deployed during the field campaign. These aerosol instruments include a TSI 3321 Aerodynamic Particle

Sizer (APS 3321), a TSI Scanning Mobility Particle Sizer (SMPS, composed of TSI parts 3082, 3083, 3750, and 3088), as well as a Handix Scientific Portable Optical Particle Spectrometer (POPS). These instruments were located in the mobile laboratory, approximately 1.7 miles from the site of drone flights, where they sampled through a vertical inlet system intaking air approximately 4 m above ground level.

The instrumentation employed measures diameter using different physical approaches, which can result in measurements that are not directly comparable. The POPS and Alphasense OPCs utilize optical measurements, which depend on the refractive index of the measured particle and classify particles by their optical diameter. The SMPS separates particle size based on electric mobility, producing a mobility diameter. The APS measurements rely on aerosol aerodynamic properties, and produce an aerodynamic diameter. Accurately comparing these different diameters requires knowledge of particle shape factor, refractive index, and density, which are not directly measured in the field. To reconcile these differences and express aerosol size distributions in terms of a geometric size distribution, POPS, APS, and SMPS data were merged to produce a best-estimate geometric size distribution using the methods described in Malm et al. 2024.

In addition to the mobile laboratory instrument package, a WideBand Integrated Bioaerosol Sensor (WIBS-neo, Droplet Measurement Technologies) was utilized for the measurement of fluorescent particles. The WIBS was located approximately 30m away from the mobile laboratory, mounted on the NEON tower 8m above the surface. It nominally detects particles from 0.5-30μm in optical diameter. The WIBS utilizes three different channels to measure particle fluorescence: emission at 310-400 nm from excitation at 280 nm (channel A), emission at 420-650nm from excitation at 280 nm (channel B), and emission at 420-650nm from excitation at 370nm (Channel C). These channels have been selected for the excitation of biological fluorophores, and fluorescent particles can be considered to be likely biological in origin (Kaye et al. 2005). As the WIBS contains three unique fluorescence channels, there exist 7 possible combinations of fluorescence channels. These are denoted as ABC if a particle fluoresces in all 3 channels, AB if a particle only fluoresces in channels A and B but not C, A if a particle fluoresces only in channel A, and so on. This classification system was first described in Perring et al. (2015). For the

purposes of this paper, particles measured by the WIBS are sorted into super micron and submicron categories, and fluorescent and non-fluorescent types.

To supplement bioaerosol fluorescence data, pollen and fungal spores were collected using a volumetric spore trap, using the methodology similar to that outlined in Hughes et al. (2020), supplemental information. In short, airborne particles are impacted on greased microscope slides. After impaction they are then dyed for visibility and counted manually using a microscope. Particle counts were then converted into approximate particle concentrations with 30-minute time resolution.

2.5 Meteorological Instrumentation

Meteorological data were collected using a surface station, (AIO Weather Sensor, Climatronics Corp.) and radiosonde measurements. The surface monitoring station was used to calibrate the iMet-4 radiosonde instrument package. Once the radiosonde balloon was sufficiently filled with helium it was released to measure meteorological variables throughout the whole atmospheric column. Similar to UA flights, radiosonde launches were conducted during quiescent conditions as well as conditions both immediately before and after cold pool passage when possible.

2.6 Data Processing

Though the OPCs sample at 1Hz, statistical considerations necessitated integrating over longer sampling periods. Namely, OPC data were averaged for the duration of the time the drones remained stationary in column formation, which, based on battery life, was typically 10-20 minutes. The drone OPC particle data were then compared to surface measurements averaged over the same time period.

Via the Shapiro-Wilk statistical test, we determined that the noise of OPC measurements during background periods tended to have a Gaussian distribution. Thus, the OPC data were analyzed using Gaussian statistics. As discussed above, the operations of the BACS campaigns led to periods in which UA-mounted and surface-mounted OPCs were all co-located in-between flight periods. These periods were then considered “baseline” periods for calibration. For each flight, if a suitable baseline period existed, the mean and standard deviation (**σ**) of particle number concentrations during that period were

calculated separately for both super- and submicron channels, and its sigma-to-mean ratio used as the error estimate of corresponding flights, and is shown as the error bars of figures such as Figure 3.4.

Sensor drift was a significant issue that required correction for each measurement period during these experiments. We utilized OPC statistics from baseline periods taken every day during the campaign to correct in-flight data if individual UA-mounted OPCs diverged from the surface measurements during those background periods. Background periods were selected from periods where all UA were outside, turned on, and sampling during a quiescent period before or after flights. The mean counts of the UA-mounted OPCs were then compared to data from the surface OPC(s), or from the merged size distributions in their absence, via a student's t-test. Data from the surface-based OPCs were prioritized over merged size distribution measurements for this comparison due to their proximity and the matching measurement technique and size range, although we show below that merged size distribution comparisons still produced high-quality data. Baseline periods were selected to be at minimum twenty minutes in length to obtain robust statistics, and at maximum one hour, while ensuring the data averaging occurred over periods with stable aerosol concentrations. while also avoiding changes in ambient aerosol.

If the t-test determined that OPCs were statistically different ($p < 0.05$) from one another during this baseline period, the drone OPCs were then corrected to the surface measurement using a constant factor to correct average particle concentrations of drone-mounted OPCs to ground OPC measurements, applied to both the background and flight periods. If no suitable baseline period existed (usually due to rain or other severe weather) no correction to average concentration was applied, and a conservative estimate for error based on OPC measurements from other days was used. In this case error bars of 30% for submicron aerosol concentrations and 50% for supermicron concentrations were utilized as they were larger than >80% of the backgrounds measured.

In cases lacking surface OPC data, profiles were supplemented with previously described merged size distributions. A method was devised to test the compatibility of OPC and merged size distribution measurements. This was particularly relevant for a period of prolonged surface OPC outage during BACS-II, 6/10/2023 - 6/12/2023. Though the surface-based OPCs were not available during this time,

UA-mounted OPCs could be utilized for direct comparison to merged size distributions during periods in which the UAs were grounded. In both the submicron and supermicron range, the largest bins in which the nominal diameter of the OPC and merged size distribution overlapped were selected. Then, lower bins were added successively and correlation analysis performed until the optimal lowest bin was found based on both measurement agreement (slope) and r-statistic [Supplemental Figures 1S and 2S]. For both submicron and supermicron measurements it was found that the use of equivalent nominal diameters of the OPC and merged size distribution yielded both robust correlations and counting efficiencies near unity, so it was decided to supplement OPC data with merged size distributions in equivalent nominal diameter space.

CHAPTER 3: RESULTS

3.1 BACS Observation Overview

Across two phases of the BACS field campaign, a wide variety of meteorological and aerosol conditions were observed, and the environmental conditions differed markedly between the two years. BACS-I began with unseasonably cold conditions, with IOP 1 on 5/24/2022 having a high temperature of only 12°C. However, as the campaign went on, the typical conditions became hot and dry. Precipitation was rarely observed during BACS-I; throughout the whole campaign period, only five precipitation events were observed, three of which were during IOPs.

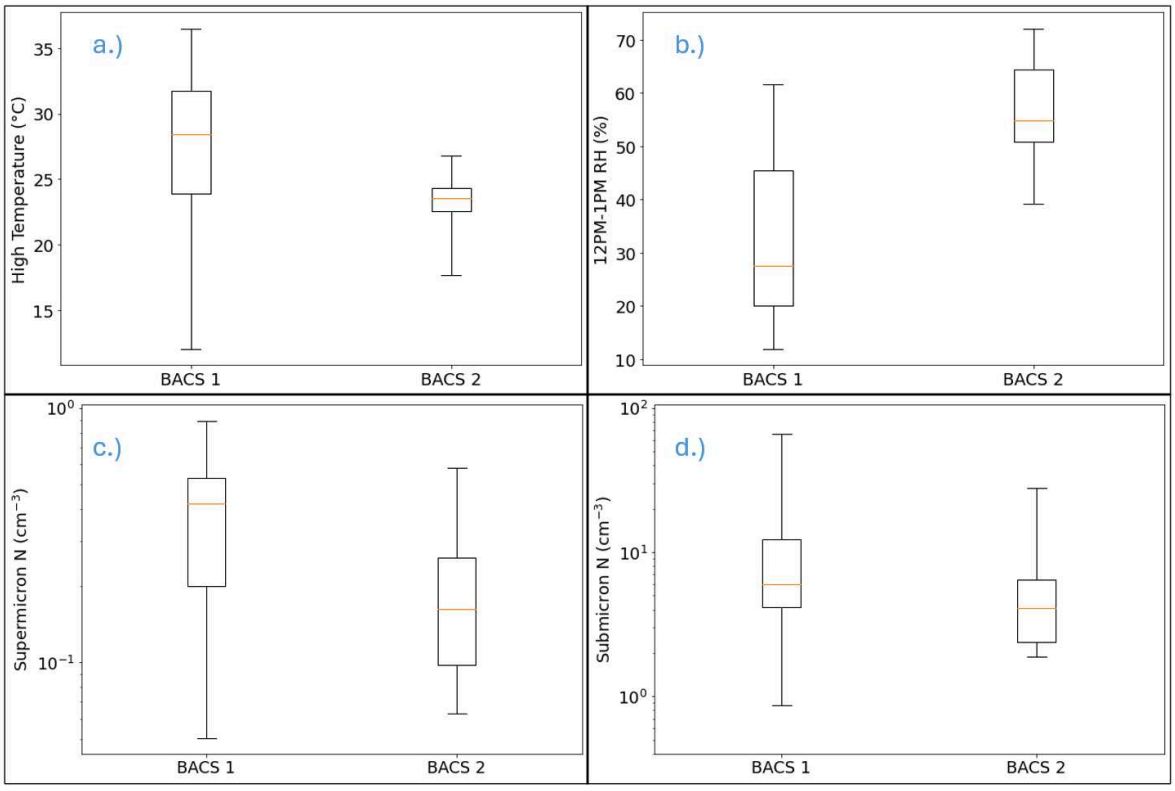

Figures 3.1a-d: Box-and whisker plot of (a) daily high temperatures; (b) average RH from 12:00PM-1:00PM; (c) average supermicron and (d) average submicron particle concentrations from 12:00PM -1:00PM, for IOPs during both periods of the BACS field campaign. Boxes represent the

interquartile range, with the horizontal orange line representing the median value. Whiskers indicate the minimum and maximum values recorded.

In contrast, conditions during BACS-II were cooler and more humid. During BACS-II, precipitation at the site was frequently brought by both mesoscale stratiform precipitation and convective storms causing both rain and hail. In total, precipitation of some kind was recorded on 20 separate days, including during several IOPs. Figures 3.1a and 3.1b show the high temperatures and relative humidities between 12:00 PM and 1:00 PM local time of both campaign periods.

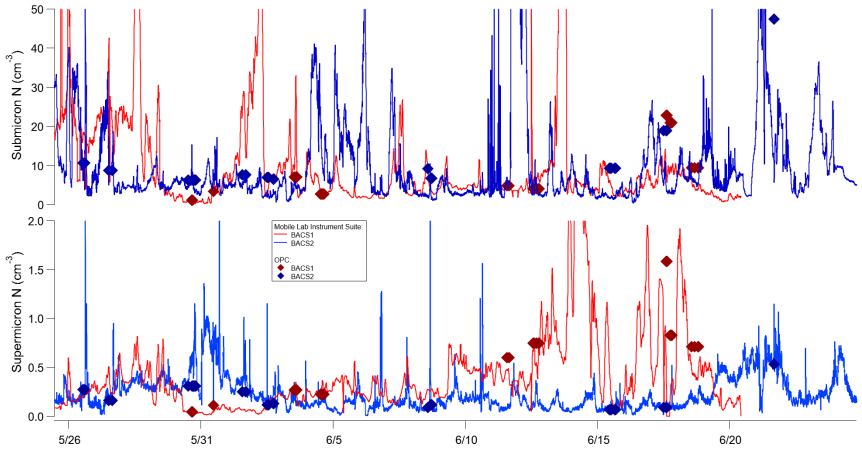

Figure 3.2: Five-minute averaged supermicron (bottom) and submicron (top) aerosol concentrations as measured by both the mobile lab instrument suite (lines) and ground-based OPCs (markers) during BACS-I (2022, red) and BACS-II (2023, blue).

The BACS field campaigns, in addition to encompassing a wide variety of meteorological conditions, also documented a diverse array of aerosol environments. BACS-I IOPs had average supermicron and submicron aerosol concentrations of 0.42 and 6.0 cm^{-3}, respectively, while for BACS-II the corresponding values were 0.16 and 4.1 cm^{-3}. Background submicron aerosol concentrations as high as 66 cm^{-3} and as low as 0.86 cm^{-3} were recorded. Variations in meteorological parameters such as precipitation and RH created a myriad of unique sampling conditions. Additionally, the field campaign detected potential influence of long-range aerosol transport, including wild-fire smoke and Saharan Dust, though these events are not presented in detail in this work.

3.2 Environmental Measurement

A goal of every IOP was to arrive at the field site to observe quiescent conditions before the development of cold pools or other mesoscale meteorological features. For the purposes of this paper, "environmental" measurements refer to the first measurements of a given type taken in an IOP, as long as those measurements are quiescent, i.e. prior to the influence of cold pools and convective storms. These environmental measurements included radiosondes and aerosol vertical profiles. A common pattern of aerosol profiles observed in BACS was a well-mixed quiescent profile (i.e., one that follows the dry adiabat), that was perturbed by the onset of convective storm dynamics (Figure 3.3).

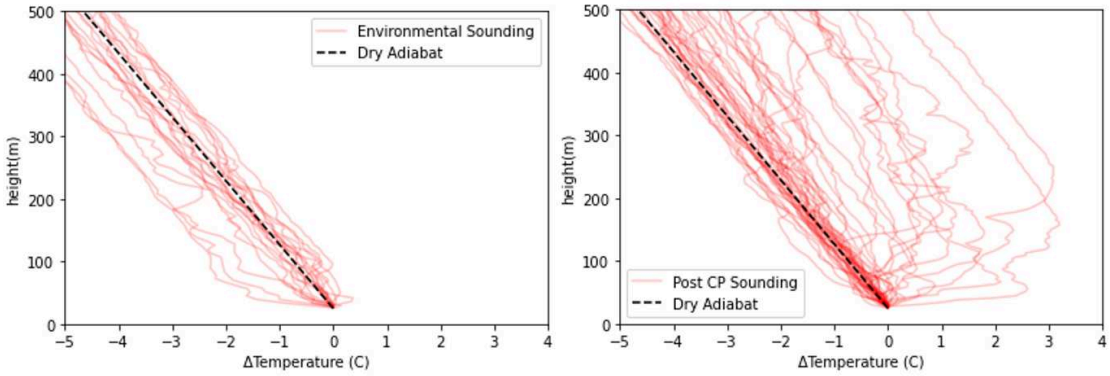

Figures 3.3a-b: Radiosonde height vs. change in temperature from 25m in (a) environmental and (b) post cold-pool measurements across both BACS-I and BACS-II. Dashed line is the dry adiabat, for comparison.

The soundings corresponding to these quiescent environmental aerosol profiles, shown in Figure 3.3a, tended to display either unstable boundary layers - lapse rates greater than the dry adiabatic lapse rate, or at the least positive temperature lapse rates, i.e. temperature decreasing with increased height. This indication of instability in the environment was to be expected, as sonde measurements were conducted on days for which convective storms were likely to develop.

Post-cold pool soundings (Figure 3.3b), on the other hand, displayed much more stable atmospheric conditions. In contrast to environmental soundings, many show temperature inversions within the region the drones flew. These perturbations from the well-mixed environmental soundings, also caused aerosol profiles to no longer be mixed. Here, an aerosol profile was defined as "well-mixed" if observations at all four heights (ground level, 120m, 235m, and 350m) agreed within expected variability due to counting statistics and measurement uncertainty, as described in methods.

Out of 28 IOPs spread across both field campaigns, environmental aerosol profiles were collected in 21. Of these 21 profiles, 16 were well-mixed in both the submicron and supermicron measurement channels, and the other 5 were well-mixed in one. This is a much higher frequency of well-mixed flights than is found in non-environmental sampling, which consisted of 64 flights, only 36 of which were well-mixed in both channels, while 14 were not well-mixed in either.

3.3 Aerosol Layers

A common feature observed in BACS aerosol profiles was elevated submicron particle concentrations measured at the 120 meter level as compared to 255m, 350m, and the surface. For the purposes of this paper, an elevated aerosol layer at 120m means that the submicron aerosol concentrations were measured to be >50% greater at 120m than the surface, and that this difference was statistically significant ($p \leq 0.05$). This feature was observed 23 times throughout BACS. It was only observed 3 times during environmental flights, making up 14% of that type, but made up 31% of non-environmental flights, and was typically observed after the passage of a cold pool or some other boundary. Figure 3.4 shows several examples of elevated aerosol concentrations appearing after the passage of a cold pool or other boundary.

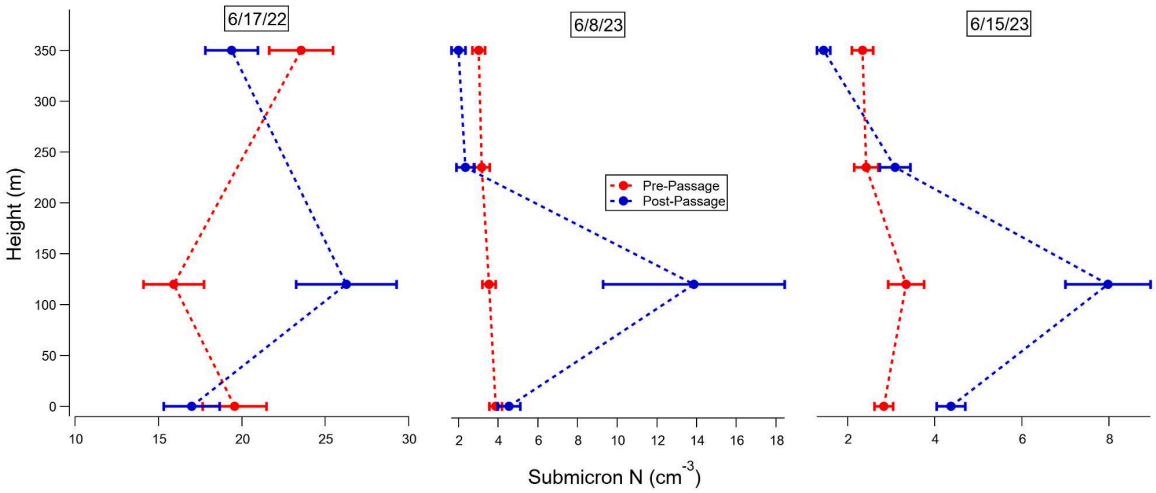

Figure 3.4: Selected submicron aerosol vertical profiles demonstrating changes caused by the passage of a cold pool or other boundary

This layer of enhanced aerosol after cold pool passage is, to the best of the authors' knowledge, not found in any cold pool literature from either an experimental or modeling perspective. Aerosol vertical gradients have many potentially important implications. Some portion of aerosol aloft will be ingested into clouds where they can act as CCN or INP, so understanding how particles are distributed throughout the vertical column is crucial to understanding their impacts on meteorological development. Three case studies (one from BACS-I, two from BACS-II) displaying this feature at 120m were selected for further analysis, to shed light on its potential causes and evolution.

3.4 Case Study 6/2/23

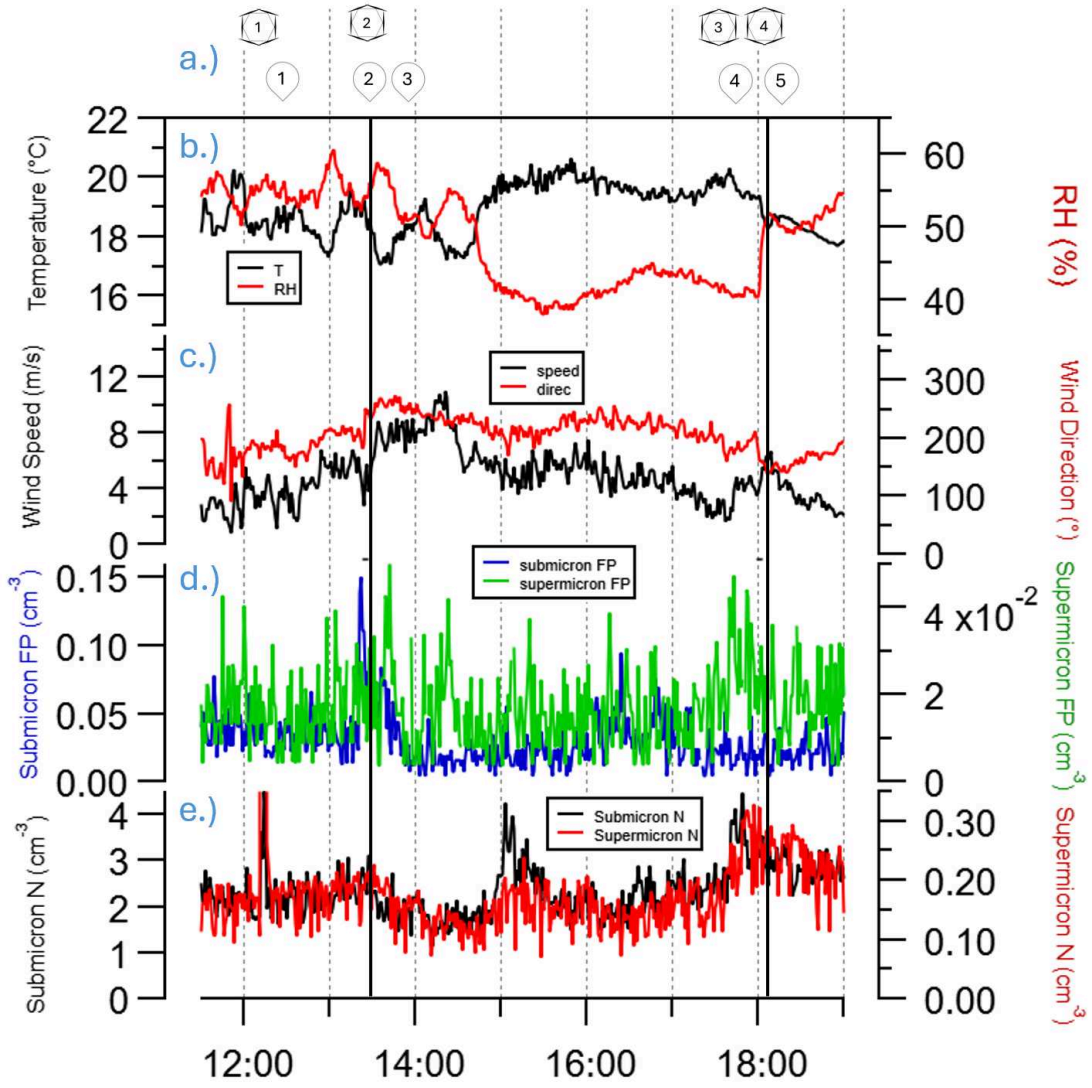

Figure 3.5a-e: Timelines of meteorological variables, surface based merged aerosol data, and drone and sonde operations during the 2 June 2023 case study. Black vertical lines mark passage of cold pools. a.) Balloon shapes mark time of radiosonde launch, while hexagonal shapes represent drone flights. b.) Temperature (left, black) and RH (red, right) measured by the surface station. c.) Wind speed (left, black) and direction (from North) (red, right) measured by the surface station d.) submicron (left, blue) and supermicron (right, green) FP measured by the WIBS-neo e.) Submicron (left, black) and supermicron (right, red) from the merged size product

During the IOP of 6/2/2023 aerosol and meteorological data were recorded over the course of several hours, capturing the passage of two distinct cold pools.The IOP began with relatively clean aerosol backgrounds, as measured by both the PurpleAir monitoring network, with the nearest sensor

reading 0 μg m^{-3}, and aerosol instrumentation deployed at the field site measuring average supermicron concentrations of ~0.15 particles/cm^3 and submicron concentrations of ~2 particles/cm^3 (Figure 3.5e). Rainfall from the previous day caused particularly humid conditions: a temperature of 14 ºC with a RH of 75% was recorded at the field site at 9:00 local time.

Between 12-12:30 environmental measurements were performed. These included stacked drone flight #1 as well as radiosonde launch #1 (Figure 3.6). The environmental aerosol profile (Figure 3.7, red) was characterized as well-mixed for both the submicron and supermicron total aerosol number concentrations, with moderate measured concentrations ranging from 2.5-4 cm^{-3} and 0.1- 0.2 cm^{-3}, respectively. The temperature profile measured by radiosonde #1 (Figure 3.6) displayed a smooth lapse rate similar to the dry adiabatic lapse rate, explaining the mixing in the aerosol profiles.

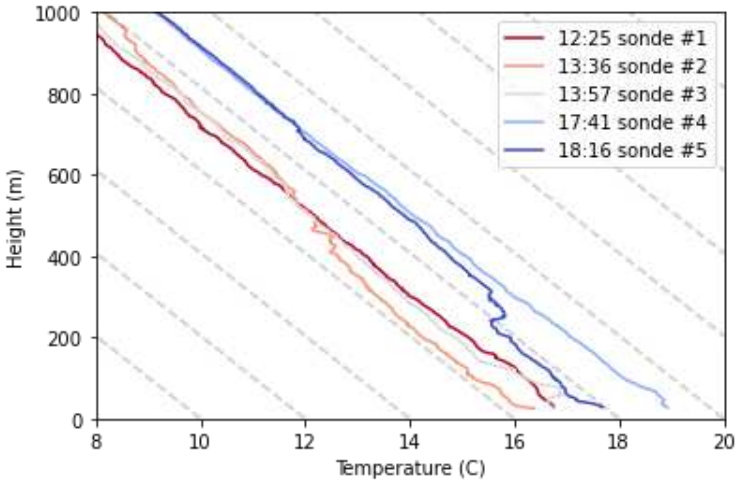

Figure 3.6: Temperature profiles measured by radiosondes for 6/2/2023. Gray lines are dry adiabats

At 12:50 it was noted that very light rain was falling at the field site, but no precipitation was recorded by the rain gauge. Around this time radar measurements suggested a convective cell was forming in the immediate vicinity of the field site. A cold pool was observed to be approaching from the west, prompting preparations for another set of sampling. Drone flight #2 began at 13:23, as indicated in Figure 3.5a. Just as the drones entered their column formation at 13:25 a rapid change in wind speed and

temperature indicated the passage of a cold pool. Another radiosonde was launched at this time, near the cold pool edge.

Coinciding with the arrival of this cold pool, a sharp increase in the number concentration of submicron fluorescent particles was observed at the surface (Figure 3.5e), while the total aerosol concentration measured by the surface OPCs was within 25% of the pre-cold pool values. However, the OPC stationed at 120m measured 6.4 cm^{-3} submicron particles, a significant ($p < 0.01$) increase in number concentration with the passage of the cold pool, and significantly higher than the other levels (235m, 350m) (Figure 3.7, pink)

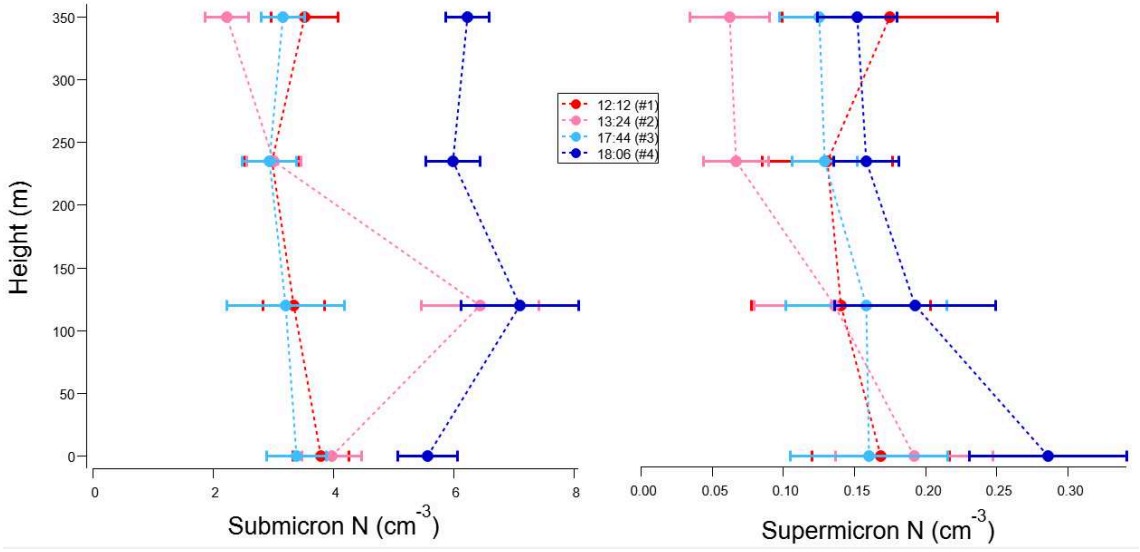

Figure 3.7: Aerosol vertical profiles in supermicron and submicron channels observed during four flights on 6/2/2023

Different explanations for the development of this layer of enhanced aerosol were considered. One possible explanation proposed was rapid deposition of aerosol at the surface after the passage of the cold pool increased aerosol concentration throughout the lower boundary layer. However, utilizing time series data, (Figure 3.5e) it does not appear that the surface aerosol concentrations were affected by cold pool passage at all. The minute-resolved aerosol concentrations of the drone-mounted OPCs, however, tell a different story. In all three OPCs, arranged in column formation, a decrease of aerosol concentration is

apparent at 13:29, followed by a sharp increase minutes later. This appears to coincide with a feature in the temperature readings aboard the UA, which show a few minutes of equilibration time (Freeman et al. 2024), followed by sharp temperature decrease in all three OPCs at approximately 13:30 (Figure 3.8).

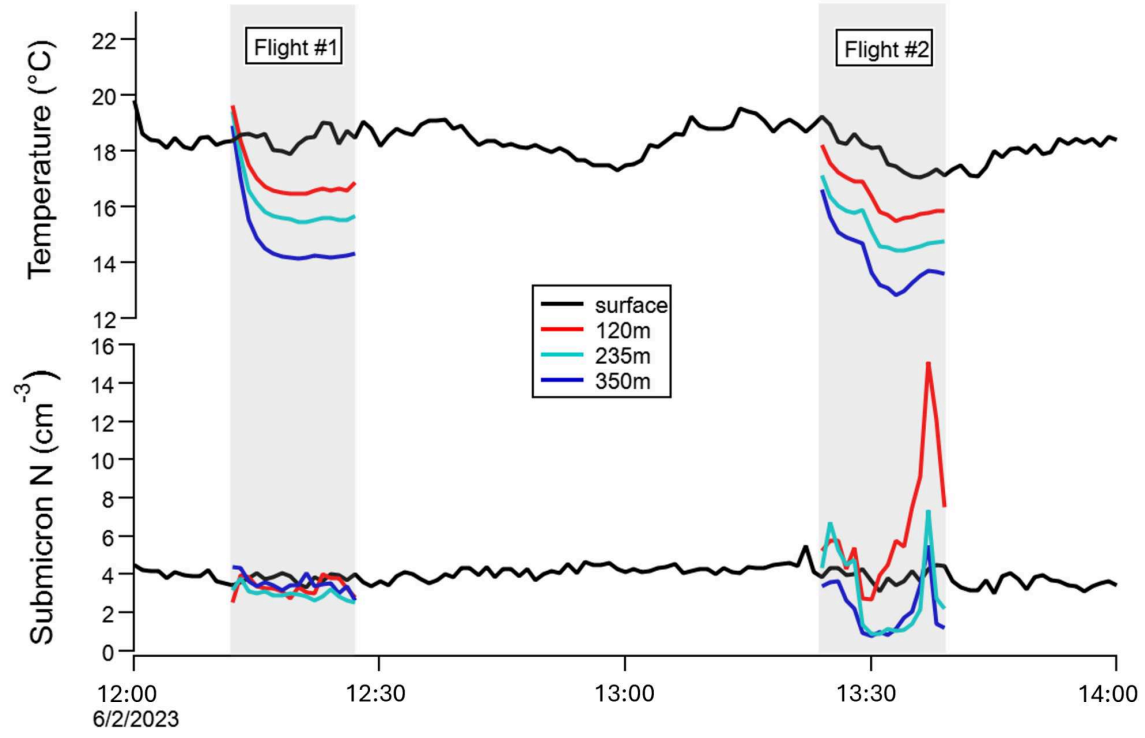

Figure 3.8: Surface and UA-mounted temperature and submicron aerosol number concentration measurements during flights 1 and 2 on 6/2/2023

The development of the aerosol profile during Flight #2 suggest that the elevated layer of aerosol at 120m is not caused by particle deposition, but may be caused by the dynamics of the cold pool itself. It appears that as a colder, higher RH (Figure 3.5b) air mass passes the site, the aerosol profile around the site changes rapidly. These changes are not evident at the surface, and so surface-based processes such as aerosol lofting by the passage of the cold pool or deposition do not offer sufficient explanations for the observation. Rather, the changing aerosol environment may be introduced by the new airmass traveling over the site.

After these measurements, several hours of quiescent conditions passed as the forecasting team looked for signs of developing cold pools. Eventually signs of an approaching cold pool were observed

and pre-cold pool radiosonde and stacked-drone measurements were taken. The aerosol perturbation at 120m did not persist at the site over four hours, as the aerosol profile for flight #3 (Figure 3.7, light blue) was found to be once again well-mixed and within 25% of values recorded during quiescent measurements at the start of the IOP.

The cold pool passed the field site at 18:01; drones took off and were oriented in stack formation by 18:06. The aerosol profile of flight #4 (Figure 3.7, dark blue) showed significantly elevated submicron particle concentrations compared with the previous quiescent measurements, as well as, once again, submicron concentrations at 120m significantly ($p = .02$) higher than those at the surface. Supermicron particles, on the other hand, were well-mixed throughout the column.

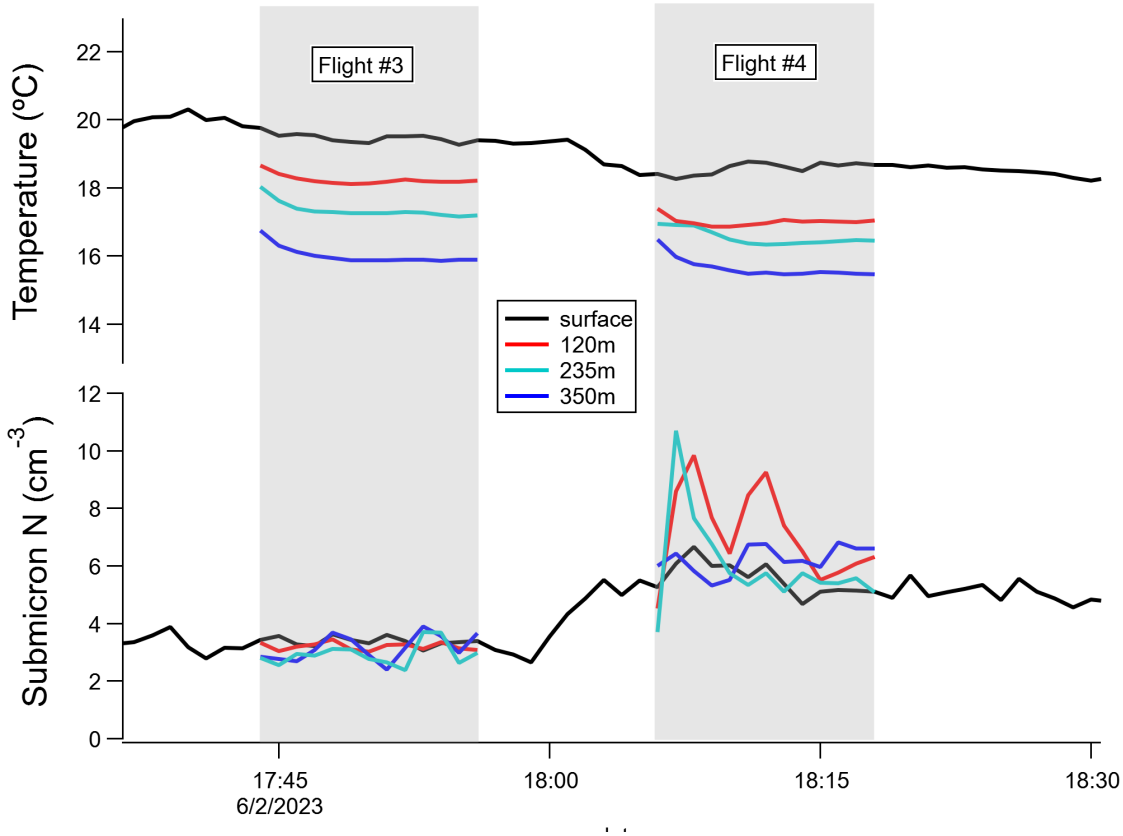

Figure 3.9: Surface and UA-mounted temperature and submicron aerosol number concentration measurements during flights 3 and 4 on 6/2/2023

This case shows a clear increase in aerosol throughout the whole column, at approximately the time of cold pool passage, ~18:00. However, a spike in fluorescent particles is only noticeable in the

submicron range. This suggests that this case is an example of cold pool lofting of nonfluorescent mineral dust, as in a haboob. There is also a spike of supermicron particle concentration at the surface during this time, which was not observed in the previous cold pool, which may also suggest the lofting of dust. The submicron aerosol profiles taken shortly after the passage of this cold pool (Figure 3.7, dark blue) show a similar aerosol environment throughout the column, suggesting that the incoming cold pool head is distributes aerosol throughout the whole column to a height of 350m,, and that any emissions from the surface are readily mixed throughout it..

This case study included two clear, successive cold pool passages and demonstrated the impacts they had on aerosol vertical profiles. During this case study, the passage of the second cold pool had minimal impact on aerosol concentrations, except at 120m, while the passage of the second cold pool raised submicron concentrations throughout the whole column, and supermicron concentrations at the surface. Neumaier (2023) proposed that the passage of a first cold pool in a pair of successive cold pools will cause more lofting of aerosol. However, the opposite appears to have occurred in this case.

Real environmental measurements obviously differ from modeled conditions in several ways. In this case, the two cold pools did not approach from the same direction, as was assumed in Neumaier (2023). The modeling study also used two identical cold pools, and that cold pools redistribute existing aerosol, but do not generate new aerosol. On this day, as the second cold pool approached from the east it interacted with an already existing boundary feature near the field site, causing it to move very slowly. The complexities of real environmental measurement make it difficult to assess the validity of modeling such as this, and the question of the effect of successive cold pool passage on aerosol vertical profiles warrants further study.

3.5 Case Study 6/3/22

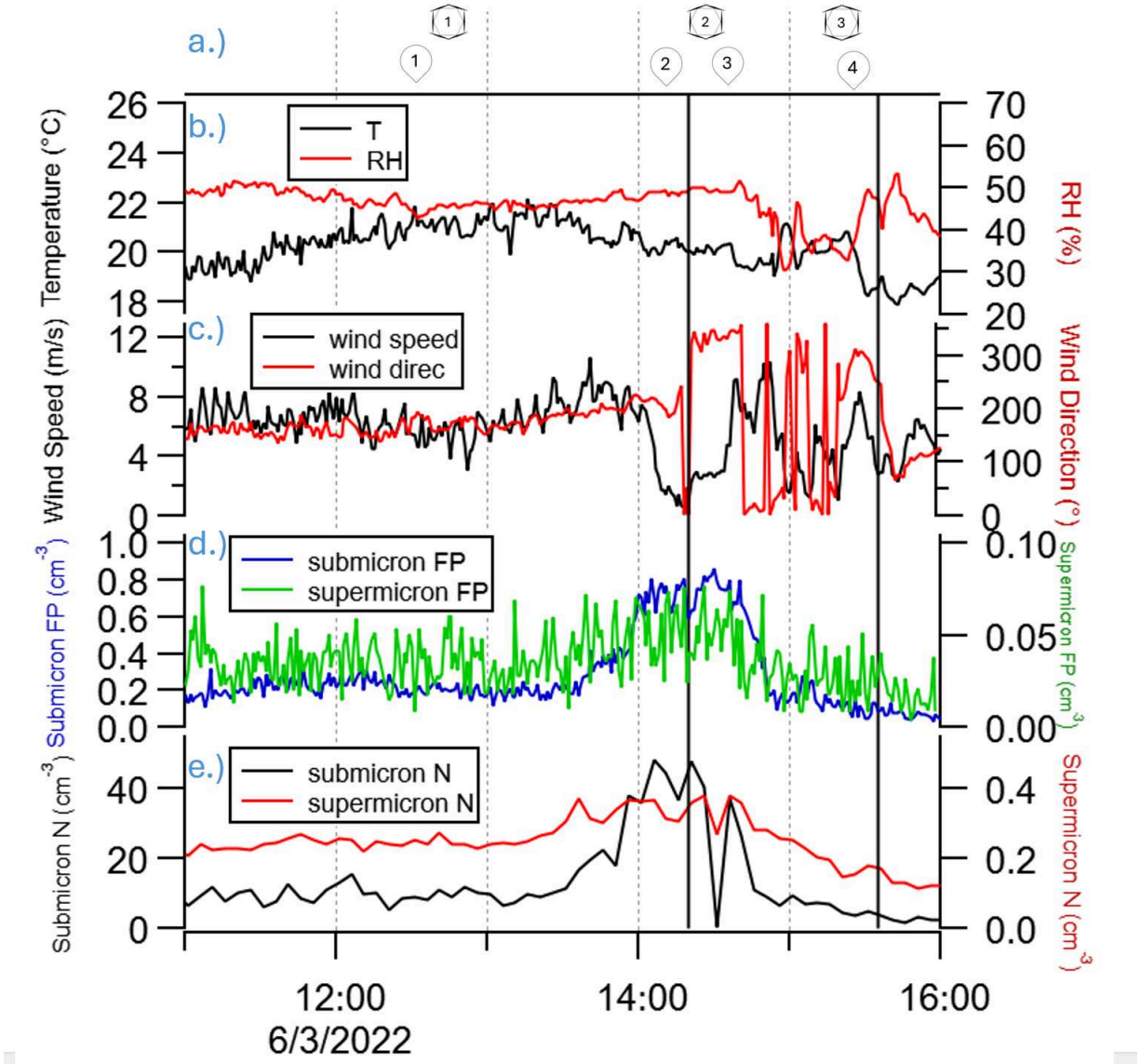

Figure 3.10: Timelines of meteorological variables, surface based merged aerosol data, and drone and sonde operations during the 3 June 2022 case study. All panels are marked as in Figure 3.5

The IOP of 6/3/2022 consisted of several hours of measurement including three stacked UA flights and four radiosonde launches. Two cold pool passages were observed, though only the first was studied as severe weather prohibited drone or radiosonde sampling of the second. Besides demonstrating elevated submicron particle concentrations at 120m in one flight, this IOP was selected for further discussion due to a surge of bioaerosol that happened during it, as discussed further below. These aerosol

layers may give important insights into the generation or transport of these submicron fluorescent particles.

The IOP began at 12:25 with environmental measurements, beginning with a radiosonde launch, and followed by a stacked drone flight at 12:41 (Figure 3.11, red). This environmental profile showed a relatively clean and well-mixed column, with supermicron and submicron particle concentrations ranging from 0.20-0.26 cm^{-3} and 6.5-8.8 cm^{-3}, respectively. Radiosonde measurements showed temperature lapse rates within the low boundary layer were similar to the dry adiabatic lapse rate. This suggests vertical lifting of air from the surface, perhaps explaining the well mixed aerosol profiles.

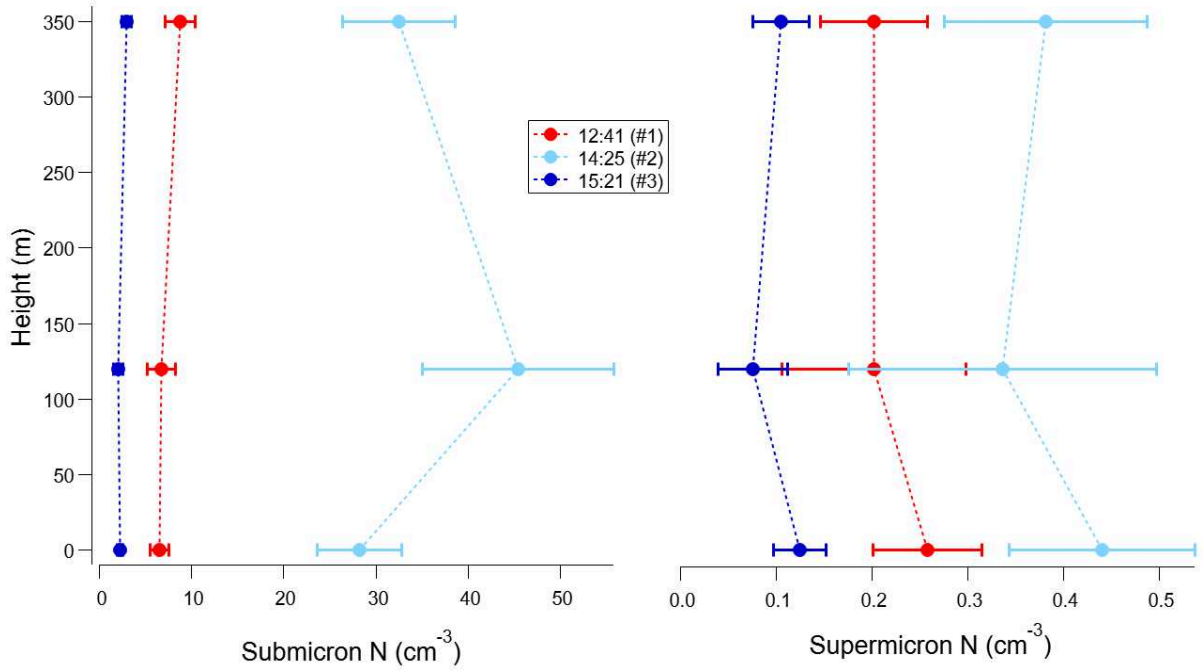

Figure 3.11: Aerosol vertical profiles in supermicron and submicron channels observed during three flights on 6/3/2022

Radar observers forecasted an approaching cold pool, so preparations were made for sampling. Surface measurements from the mobile laboratory (Figure 3.10e) during the period between the environmental and passage flights showed a rapid increase in aerosol concentrations at approximately 13:50, before the arrival of precipitation at the site. At the same time, the WIBS measured a large increase in fluorescent aerosol.

The measured fluorescent particles were primarily identified as B- or BC-type particles, which could be pollen fragments (Hughes et al., 2020), among other things. Over the course of this IOP, B- and BC-type fluorescent submicron particles combined to make up ~95% (Figure 3.12) of all detected submicron fluorescent particles. The large increase in number concentrations of these particles are consistent with the release, and then rupture, of pollen grains. During this time, the pollen collected by the spore trap also increased (Figure S3). Between 10:01 AM- 13:01 only 9 pollen grains were collected (35 m^{-3}), while from 13:01 - 16:01 this frequency doubled, and 18 pollen grains were counted (70 m^{-3}). One ruptured pollen fragment was observed collected over this time period.

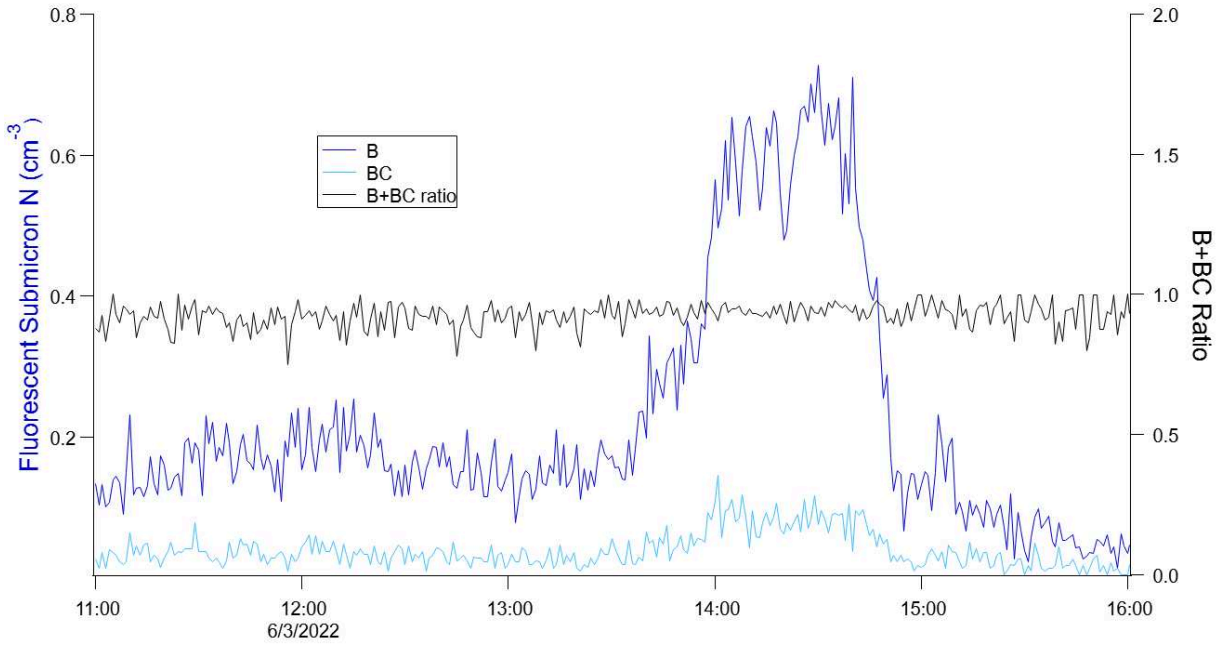

Figure 3.12: Concentrations of submicron fluorescent particles of B- and BC- type (blues, left) and fraction of B- and BC- type fluorescent particles compared to total submicron fluorescent particles (black, right)

Contrary to the hypothesized pollen rupture, the RH measured at the surface for the duration of this IOP, 40-50%, are much lower than those reported necessary for the rupture of types of pollen studied previously (Taylor et al. 2004). Pollen may rupture for other reasons, such as collision with a solid surface

(Visez et al. 2015), though it is unclear how significant a role these processes play in the real environment. A large increase in submicron fluorescent aerosol beginning at ~13:30 was observed, though the fraction of submicron fluorescent particles as a total of total submicron particles remained approximately constant. The rupturing of pollen grains into SPP may not sufficiently explain this. Previous literature has also observed B-type fluorescent particle concentrations being well-correlated with total particle concentrations, suggesting a similar source for fluorescent particles as other non-fluorescent particles (Yu et al. 2016). Previous literature has also shown that this type of fluorescent particle is associated with non-biological particles including humic-like substances and burning emissions (Yue et al. 2022) though it is unclear whether this may be due to particles of mixed-biological origin.

A pre-cold-pool sonde (#2) was launched at 14:10. At 14:20 shifting winds indicated that a cold pool had indeed passed the field site. Shortly after this, the drones reached their column arrangement and sampling began. The profile flight after the passage of this cold pool (Figure 3.11, light blue) demonstrated increased aerosol concentrations throughout the column, as well as significantly ($p = .02$) elevated submicron concentrations at 120m as compared to the surface.

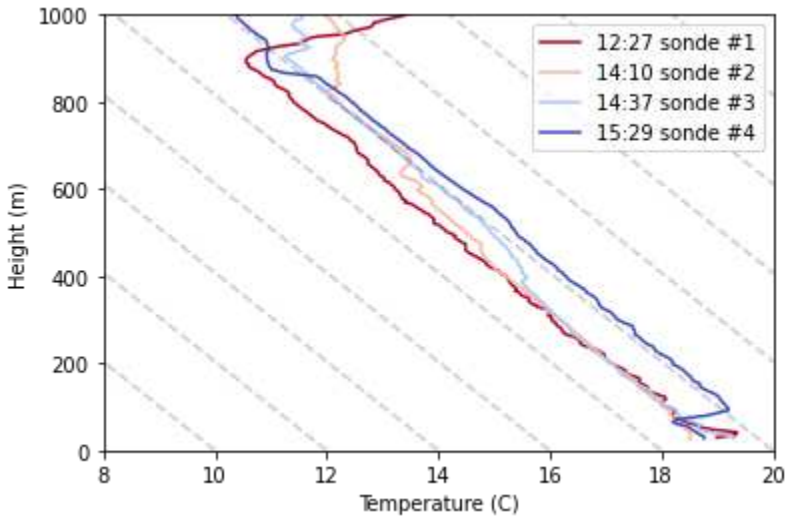

Figure 3.13: Temperature profiles measured by radiosondes for 6/3/2022

After the rain let up, another round of sampling was conducted. Drones flew in post-cold pool conditions (Figure 3.13, dark blue), but based on changes in wind speed and direction during the flight, may have captured the passage of a second, weaker cold pool. Perhaps due to the rain, this flight measured a well-mixed aerosol profile, with lower concentrations throughout the whole column than in the previous flight with submicron aerosol concentrations ranging from 2.1-3.0 cm^{-3} and supermicron from 0.08-0.12 cm^{-3}. The observations represent a reduction in number concentration, compared with the previous flight (#2) that day, of 90% in submicron and 50% in supermicron particles. Some component of this reduction could be due to wet deposition processes removing aerosol, or detrainment of clean free tropospheric air into the cold pool.

3.6 Case Study 6/10/23

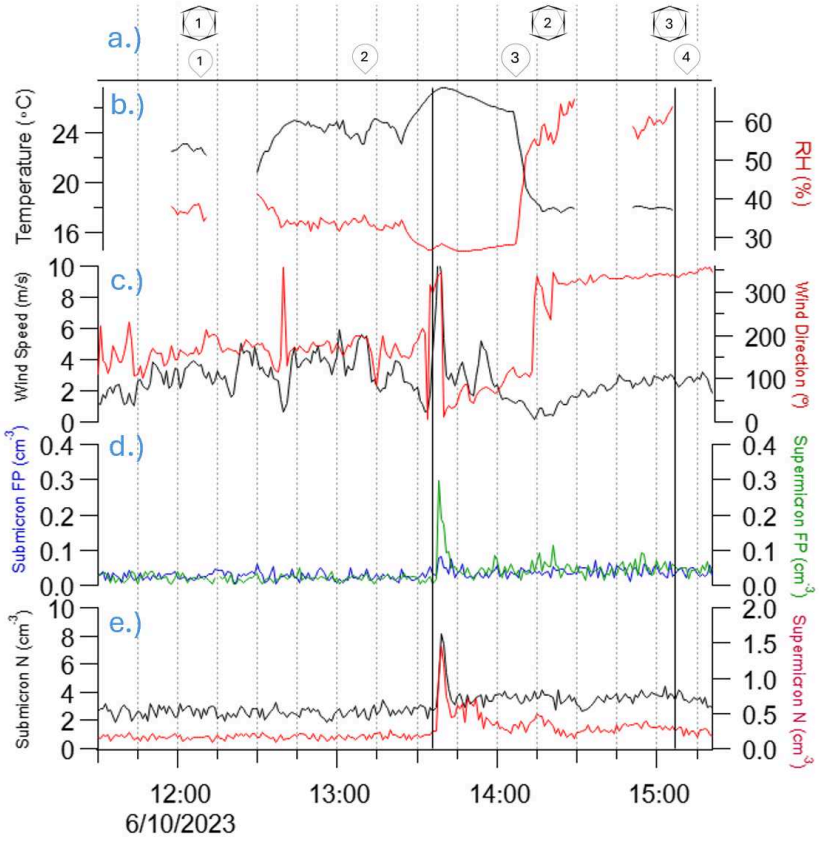

Figure 3.14: Timelines of meteorological variables, surface based merged aerosol data, and drone and sonde operations during the 3 June 2022 case study. Balloon shapes mark time of radiosonde launch, while hexagonal shapes represent drone flights. Black vertical lines mark passage of cold pools. An instrument outage caused the loss of RH data from ~13:30-14:15

The day of Saturday June 10th 2023 began with clean aerosol backgrounds across Northern Colorado, according to PurpleAir monitoring data, with the nearest sensor reading -1 μg cm^{-3}, as well as the BACS suite of aerosol instrumentation, measuring approximately 0.15 cm^{-3} supermicron particles. Weather conditions and forecasts looked promising for cold pool development. Forecasting models predicted cold pools to reach the field site in the early afternoon. The site was considered to be at marginal risk for severe weather. Based on these conditions, it was decided to conduct an IOP.

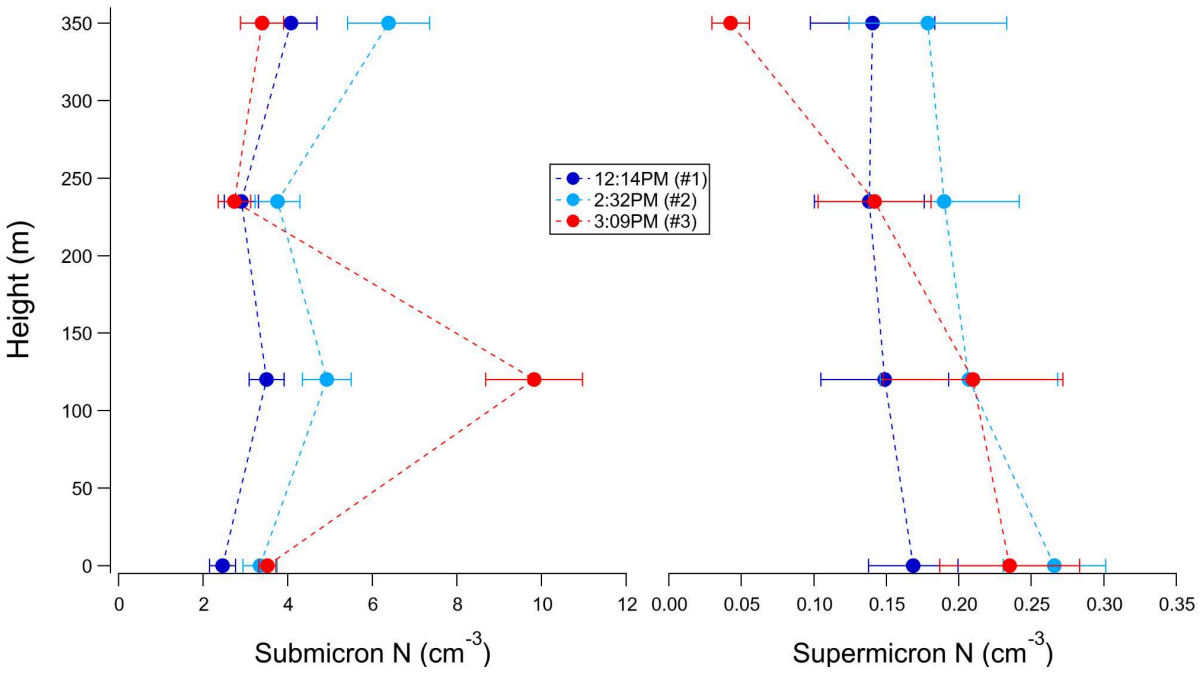

Figure 3.15: Aerosol vertical profiles in supermicron and submicron channels observed during three flights on 6/10/2023

As soon as the team arrived at the field site, environmental sampling was performed. At 12:12 the drones were flown for their first set of sampling. During this flight, at 12:21, the environmental radiosonde was launched for the environmental flight. This flight measured a relatively clean and well-mixed boundary layer, with submicron concentrations ranging between 2.9-4.1 cm^{-3}, and supermicron from 0.13-0.15 cm^{-3}. For the entirety of this day, surface OPCs were not available due to a power supply issue. In lieu of these OPC data, merged size distribution data were used to construct well correlated proxy data, as described in the methods section.

Shortly after environmental sampling, it was noted that convection was intensifying to the northwest of the site. A convective storm quickly moved through the site, bringing with it heavy rainfall and hail, as well as a shift in wind direction to northerly. At 13:35, coinciding with this rainfall, there was

a spike in both supermicron and submicron aerosol concentrations. Additionally at this time there was a clear signal of cold pool passage as wind speed increased dramatically.

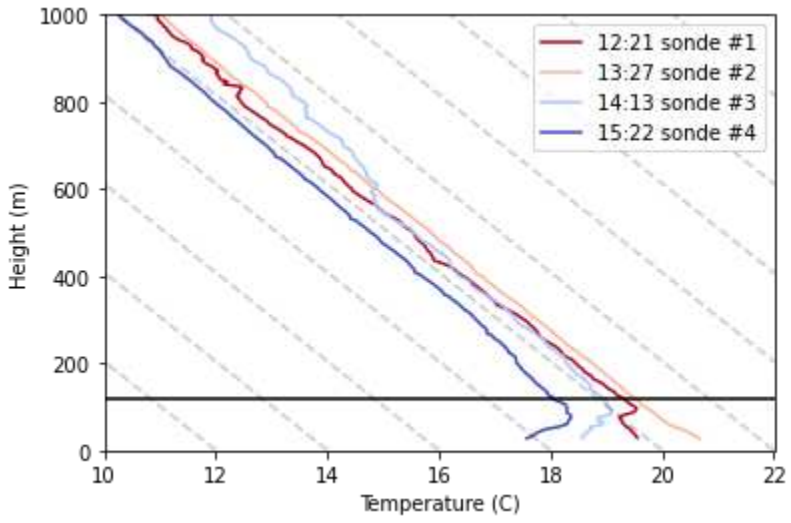

Figure 3.16: Radiosonde measurements taken on 6/10/2023. The black horizontal line marks 120m, the height of the lowest UA

Unfortunately due to the extreme weather conditions, it was impossible to capture the passage of this cold pool with either radiosonde or drone measurements. As soon as the weather allowed, post-cold pool measurements were taken, though by that point nearly an hour had passed since the cold pool reached the field site.

Radiosonde #3 launched at 14:13. At 14:30 UAs launched for post-cold pool sampling. This flight displayed aerosol concentrations that were modestly elevated from earlier environmental soundings, with ground-level submicron aerosol number concentrations as measured by the mobile lab instrument suite increasing from 2.5 to 3.4 cm^{-3} and supermicron from 0.17-0.27 cm^{-3}. Submicron particle concentrations were also raised within the column, and once again relatively well-mixed in the vertical, this time ranging from 3.8-6.4 cm^{-3}, while the supermicron channel was not significantly different from environmental measurements.

Immediately after this flight, another cold pool was seen approaching from the northwest, so another round of sampling was performed as quickly as possible. UAs took off at 15:08. The cold pool

passed at approximately 15:07 while the drones were in column formation. More measurements were conducted on this day after this first set of radiosondes and UA flights, which are not discussed in further detail in this work.

The aerosol profile from this flight (Figure 3.15, red) had significantly elevated submicron particle concentrations at the 120m drone, with this OPC reading 9.8 cm^{-3} in the submicron channel, more than a factor of 2 higher than either of the other drone-mounted OPCs or the aerosol instrument suite, and significantly greater than concentrations measured at either different altitude ($p < .01$). The supermicron profiles, on the other hand, paint a significantly different picture. At 120m, the UA-mounted OPC measured 0.60 cm^{-3}, nearly exactly the same as the pre-cold pool value of 0.61 cm^{-3}, and similar to the merged data value of 0.48 cm^{-3}, while the highest UA (350m) reported a highly clean environment, measuring only 0.04 cm^{-3}, compared to the pre cold pool value of 0.18cm^{-3}.

This profile once again demonstrates the feature of elevated submicron particles as measured at 120m. Unlike the previous case study, on this day there was not clear evidence pointing towards the presence of sub-pollen particles, as submicron fluorescent particles as a whole remained very scarce for the entire day (> 0.1 cm^{-3}). One possible explanation for elevated particle concentrations at 120m is the low inversion present at ~100m around the time of flight #3. Temperature inversions may prohibit vertical motion and trap aerosol around the height they occur (Stull, 1988).

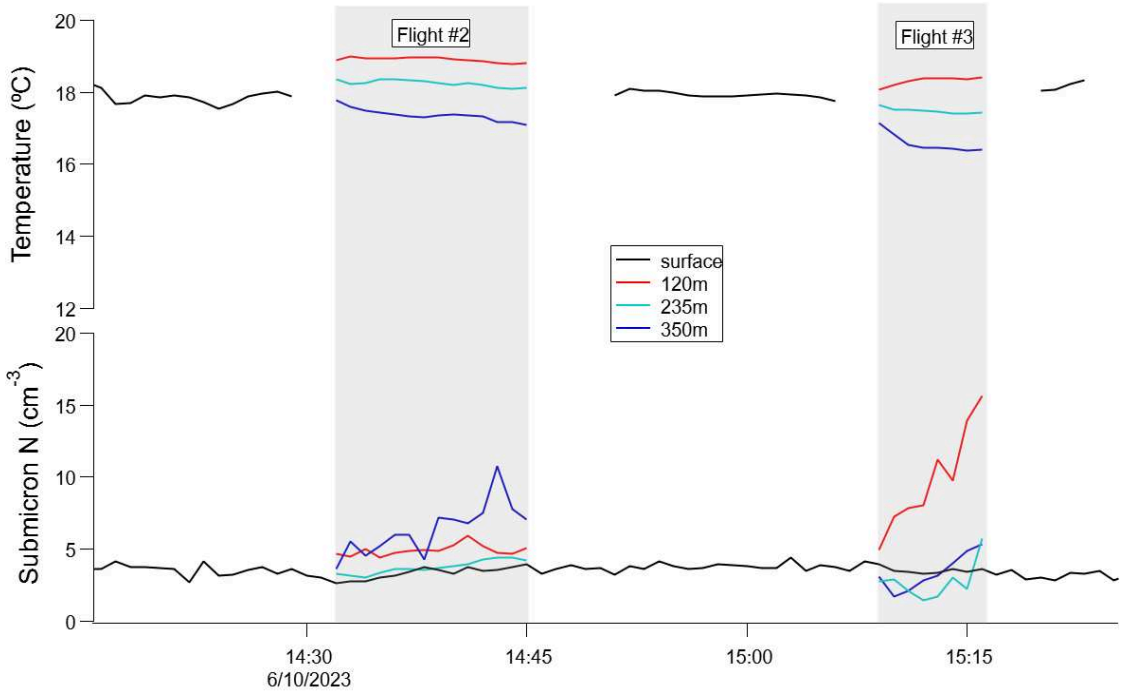

Figure 3.17: Surface and UA-mounted temperature and submicron aerosol number concentration measurements during flights 1 and 2 on 6/10/2023

However, as in the 6/2/20223 case study (Figure 3.8), once again, the concentration of submicron aerosol throughout the course of the flight appears to be dynamic (Figure 3.17). The measured concentration at the 120m drone undergoes a fairly steady increase from its beginning value of 6.1 cm^{-3} to the final concentration recorded during the flight of 16 cm^{-3} The higher two OPCs may also show an increase in concentration over the same time period. However, unlike the case study of 6/2/2023, this feature does not seem to be accompanied by any clear change in temperature measured by the UAs. In this case this may be because the passage of the cold pool at ~15:07 does not appear to have had a major impact on temperature at the surface. An unfortunate surface station outage required the use of UA-mounted iMet sensor data to supplement surface data during periods in which the drone was grounded, but the temperature is fairly constant at ~18°C both before and after passage of this cold pool.

There is also the question of the suppressed supermicron particle concentrations shown in flight #3. There was no precipitation during the flight; it did not begin until ~15:20, shortly after the UAs had

landed, so scavenging of aerosol by rain is not a likely explanation. The 350m drone is also far below the cloud base, so scavenging by cloud droplets is not a sufficient explanation either.

This case study once again seems to suggest that the enhanced layer of submicron aerosol at 120m is not caused directly by exchange with the surface, as surface submicron aerosol concentrations remained approximately constant over the course of these three UA flights. The clear increase in concentration at 120m over the course of the flight (Figure 3.15), may again suggest that the dynamics of the cold pool bring different air masses to different altitudes, causing this unique aerosol feature.

CHAPTER 4: SUMMARY AND CONCLUSIONS

A brief overview of the BACS field campaign was presented and discussed, including typical aerosol and meteorological data for the two campaign periods in 2022 and 2023 in Northern Colorado. In this study UAs were successfully utilized to study the impact of cold pool passage and aerosol vertical profiles. By flying three UAs with OPCs mounted in a column formation, aerosol profiles were obtained. Quiescent/environmental measurements were performed in addition to measurements before, during, and after cold pool passage for comparison, in order to study the effects of cold pools on the thermodynamic environment and on the vertical distributions of sub- and supermicron aerosols. With the additional support of a variety of aerosol and meteorological instrumentation, aerosol profiles were contextualized using aerosol sizing instruments as well as fluorescent particle measurements.

The challenges inherent in deploying UA-mounted instrumentation include the potential impact of rotor-induced turbulence on OPC sampling. In addition to a brief discussion of the literature surrounding this issue, an experiment was devised to demonstrate that mounting on the UA and proximity to the running propellers had little, if any, impact on its bias in measuring aerosol number concentrations in the size range discussed in this paper.

Additional challenges related to the deployment of UA-mounted OPC measurements, specific to the Alphasense OPC-N3 utilized in this experiment. Particularly, sensor drift between measurement periods was apparent and the instrument's relatively weak 5V fan introduces challenges when sampling in high wind conditions. Data processing procedures which help ameliorate these issues were developed and described.

It was found that the passage of cold pools and other boundaries often introduced a layer of elevated submicron aerosol concentration at approximately 120m into aerosol vertical profiles observed during the BACS campaigns. Possible explanations were proposed for this, including pollen rupture, emission from or deposition to the surface, and low-level temperature inversions causing the

accumulation of aerosol. These different explanations were investigated via case studies. However, none of these explanations could clearly be applied to every case. Examination of minute-averaged aerosol number concentrations throughout the course of the flights suggested that the cause of this feature may be related to the dynamics of the cold pool itself. For example, in the cases of 6/2/2023 flight #2 (Figure 3.8) and 6/10/2023 flight #3 (Figure 3.15), the aerosol concentration measured at 120m increased over the course of the flight, while aerosol concentrations at the surface remained nearly constant, strongly suggesting that the origin of this feature is not due to a surface effect, such as very local particle emission or deposition.

The examination of case studies also allowed for the investigation of several important phenomena. The case study from 6/2/2023 offered an in-depth look at the phenomenon of elevated aerosol layers at 120m. It also presented an opportunity to examine the effects of successive cold pool passage, multiple cold pools passing in one day. Comparison with a previous modeling study appeared to contradict the prediction that the first cold pool in a sequence of successive cold pools lofts the most aerosol into the atmosphere, though with the caveat that the observed conditions differed from the model parameters in several important ways.

The 6/3/2022 case study was an opportunity to examine the effects of relatively high pollen concentrations seen in pollen slide analysis. Aerosol fluorescence measurements suggested that SPPs were the potential identity of a rapid increase in aerosol concentration occurring in the afternoon of 6/3/2022. Vertical profiles as measured by UAs during this time period demonstrated that these fluorescent submicron particles were lofted throughout the heights measured by UAs, and once again may have been elevated at the 120m level.

CHAPTER 5: FUTURE WORK

This work is the first of likely many research projects relating to the BACS field campaign. Several other datasets, either briefly discussed or unmentioned so far in this paper, will eventually be integrated with and compared to the results presented in this work. For one example, aerosol filters were collected using a drone-mounted air sampler, on a UA flown at 120m during many of the other aerosol flights. DNA analysis of these filters, when complete, will give further insight into the identity of bioaerosol measured during this field campaign.

The UA mounted sampling platform devised for BACS has proven successful at measuring aerosol concentrations at different altitudes. This system has myriad potential uses. UA mounted aerosol instrumentation may be used to study cold pools in different environments, or other meteorological phenomena. UA have a variety of different use cases, as many environments are not suited to other forms of aerosol vertical profiling. The mobility and low cost of this system gives it the potential for myriad potential use cases.

One way to improve potential future experiments would be simply with the use of more OPCs. The lightweight OPCs are low cost and only have limited impact on each UAs battery life, so this is an achievable proposal. Having a larger network of OPCs could potentially decrease issues caused by sensor drift or calibration issues, as the larger number of OPCs will provide more robust statistics. During this field campaign there were also significant periods of instrument outage, so additional OPCs could ensure that at least some data were collected on each drone.

One interesting question to probe in the future could be the precise location of this layer of aloft aerosol enhancement. This work identifies enhanced aerosol at 120m in several cases, but the UAs were only stationed at the surface, 120m, 235m, and 350m, so the precise location of the maximum enhancement is unknown. An obvious way to probe this question would be to increase the number of UAs, though cost and logistics may prohibit this. More information on the vertical structure of aerosols

and how this changes with meteorology might be helpful in providing insights to the causes that shape these profiles, and their longevity as feature

REFERENCES

Altstädter, B., et al. "ALADINA–an unmanned research aircraft for observing vertical and horizontal distributions of ultrafine particles within the atmospheric boundary layer." *Atmospheric Measurement Techniques* 8.4 (2015): 1627-1639.

Andrews, E., P. J. Sheridan, and J. A. Ogren. "Seasonal differences in the vertical profiles of aerosol optical properties over rural Oklahoma." *Atmospheric Chemistry and Physics* 11.20 (2011): 10661-10676.

Augustin-Bauditz, Stefanie, et al. "Laboratory-generated mixtures of mineral dust particles with biological substances: characterization of the particle mixing state and immersion freezing behavior." *Atmospheric Chemistry and Physics* 16.9 (2016): 5531-5543.

Barry, Kevin R., et al. "Observations of ice nucleating particles in the free troposphere from Western US wildfires." *Journal of Geophysical Research: Atmospheres* 126.3 (2021): e2020JD033752.

Conen, Franz, et al. "Biological residues define the ice nucleation properties of soil dust." *Atmospheric Chemistry and Physics* 11.18 (2011): 9643-9648.

Crazzolara, Claudio, et al. "A new multicopter-based unmanned aerial system for pollen and spores collection in the atmospheric boundary layer." *Atmospheric Measurement Techniques* 12.3 (2019): 1581-1598.

Creamean, Jessie M., et al. "Assessing the vertical structure of Arctic aerosols using balloon-borne measurements." *Atmospheric Chemistry and Physics (Online)* 21.PNNL-SA-156656; BNL-221118-2021-JAAM (2021).

Creamean, Jessie M., et al. "HOVERCAT: a novel aerial system for evaluation of aerosol–cloud interactions." *Atmospheric Measurement Techniques* 11.7 (2018): 3969-3985.
Delle Monache, Luca, et al. "In situ aerosol profiles over the Southern Great Plains cloud and radiation test bed site: 2. Effects of mixing height on aerosol properties." *Journal of Geophysical Research: Atmospheres* 109.D6 (2004).

Droegemeier, Kelvin K., and Robert B. Wilhelmson. "Three-dimensional numerical modeling of convection produced by interacting thunderstorm outflows. Part I: Control simulation and low-level moisture variations." *Journal of the atmospheric sciences* 42.22 (1985): 2381-2403.

DeMott, Paul J., et al. "Predicting global atmospheric ice nuclei distributions and their impacts on climate." Proceedings of the National Academy of Sciences 107.25 (2010): 11217-11222.

Després, VivianeR, et al. "Primary biological aerosol particles in the atmosphere: a review." *Tellus B: Chemical and Physical Meteorology* 64.1 (2012): 15598.

Freeman, S. W., C. A. Neumaier, L. D. Grant, J. Bukowski, B. Ascher, N. M. Falk, B. Heffernan, G. R. Leung, R. J. Perkins, Z. Schwalbe, P. J. DeMott, S. M. Kreidenweis, E. A. Stone, and S. C. van den Heever, 2024: The Chimney: A lightweight 3D-printed, aspirated housing for measuring atmospheric thermodynamics. J. Atmos. Ocean Tech., in prep

Fröhlich-Nowoisky, Janine, et al. "Bioaerosols in the Earth system: Climate, health, and ecosystem interactions." *Atmospheric Research* 182 (2016): 346-376.

Greenberg, J. P., A. B. Guenther, and A. Turnipseed. "Tethered balloon-based soundings of ozone, aerosols, and solar radiation near Mexico City during MIRAGE-MEX." *Atmospheric Environment* 43.16 (2009): 2672-2677.

Goff, R. Craig. "Vertical structure of thunderstorm outflows." *Monthly Weather Review* 104.11 (1976): 1429-1440.

Haas, Patrick Y., et al. "Development of an unmanned aerial vehicle UAV for air quality measurement in urban areas." *32nd AIAA Applied Aerodynamics Conference*. 2014.

Holben, Brent N., et al. "AERONET—A federated instrument network and data archive for aerosol characterization." *Remote sensing of environment* 66.1 (1998): 1-16.

Huffman, J. Alex, et al. "High concentrations of biological aerosol particles and ice nuclei during and after rain." *Atmospheric Chemistry and Physics* 13.13 (2013): 6151-6164.

Hughes, Dagen D., et al. "Characterization of atmospheric pollen fragments during springtime thunderstorms." *Environmental science & technology letters* 7.6 (2020): 409-414.

Iowa State University, Iowa Environmental Mesonet, retrieved from https://mesonet.agron.iastate.edu/, 2024

Jaenicke, Ruprecht. "Tropospheric aerosols." *International geophysics*. Vol. 54. Academic Press, 1993. 1-31.

Kanji, Zamin A., et al. "Overview of ice nucleating particles." Meteorological monographs 58 (2017): 1-1.

Kaye, Paul H., et al. "Single particle multichannel bio-aerosol fluorescence sensor." *Optics express* 13.10 (2005): 3583-3593.

Kim, Man‐Hae, et al. "Quantifying the low bias of CALIPSO's column aerosol optical depth due to undetected aerosol layers." *Journal of Geophysical Research: Atmospheres* 122.2 (2017): 1098-1113.

Kok, Jasper F., et al. "The physics of wind-blown sand and dust." Reports on progress in Physics 75.10 (2012): 106901.

Kwak, Kyung-Hwan, et al. "Daytime evolution of lower atmospheric boundary layer structure: comparative observations between a 307-m meteorological tower and a rotary-wing UAV." *Atmosphere* 11.11 (2020): 1142.

Lei, Lu, et al. "Vertical distributions of primary and secondary aerosols in urban boundary layer: Insights into sources, chemistry, and interaction with meteorology." *Environmental Science & Technology* 55.8 (2021): 4542-4552.

Li, Zhanqing, et al. "Aerosol and boundary-layer interactions and impact on air quality." *National Science Review* 4.6 (2017): 810-833.
Liu, Cheng, et al. "Vertical distribution of PM2. 5 and interactions with the atmospheric boundary layer during the development stage of a heavy haze pollution event." *Science of the Total Environment* 704 (2020): 135329.

Liu, Pengfei, et al. "Aircraft study of aerosol vertical distributions over Beijing and their optical properties." *Tellus B: Chemical and Physical Meteorology* 61.5 (2009): 756-767.

Liu, Zixia, et al. "Characterizing the performance of a POPS miniaturized optical particle counter when operated on a quadcopter drone." *Atmospheric Measurement Techniques Discussions* 2021 (2021): 1-33.

Malm, William C., et al. "Revisiting integrating nephelometer measurements." *Atmospheric Environment* 319 (2024): 120237.

Neumaier, Christine Allison. *Cold Pool Train Dynamics and Transport*. MS thesis. Colorado State University, 2023.

O'Sullivan, Daniel, et al. "The adsorption of fungal ice-nucleating proteins on mineral dusts: a terrestrial reservoir of atmospheric ice-nucleating particles." *Atmospheric Chemistry and Physics* 16.12 (2016): 7879-7887.

Petters, M. D., and S. M. Kreidenweis. "A single parameter representation of hygroscopic growth and cloud condensation nucleus activity." Atmospheric Chemistry and Physics 7.8 (2007): 1961-1971.

Pringle, K. J., et al. "Global distribution of the effective aerosol hygroscopicity parameter for CCN activation." *Atmospheric Chemistry and Physics* 10.12 (2010): 5241-5255.

Pummer, B. G., et al. "Ice nucleation by water-soluble macromolecules." *Atmospheric Chemistry and Physics* 15.8 (2015): 4077-4091.

Rathnayake, Chathurika M., et al. "Influence of rain on the abundance of bioaerosols in fine and coarse particles." *Atmospheric Chemistry and Physics* 17.3 (2017): 2459-2475.

Rio, C., et al. "Shifting the diurnal cycle of parameterized deep convection over land." *Geophysical Research Letters* 36.7 (2009).

Rosenfeld, Daniel, et al. "Global observations of aerosol‐cloud‐precipitation‐climate interactions." Reviews of Geophysics 52.4 (2014): 750-808.

Rozwadowska, Anna. "Influence of aerosol vertical profile variability on retrievals of aerosol optical thickness from NOAA AVHRR measurements in the Baltic region." *Oceanologia* 49.2 (2007).

Saleeby, Stephen M., et al. "The influence of simulated surface dust lofting and atmospheric loading on radiative forcing." *Atmospheric chemistry and physics* 19.15 (2019): 10279-10301.

Steiner, Allison L., et al. "Pollen as atmospheric cloud condensation nuclei." *Geophysical research letters* 42.9 (2015): 3596-3602.

Stull, Roland B. *An Introduction to Boundary Layer Meteorology.* Springer Dordrecht, 1988

Sun, Tianlin, et al. "Time-resolved black carbon aerosol vertical distribution measurements using a 356-m meteorological tower in Shenzhen." *Theoretical and Applied Climatology* 140 (2020): 1263-1276.

Seinfeld, John H., and Spyros N. Pandis. *Atmospheric chemistry and physics: from air pollution to climate change*. John Wiley & Sons, 2016.

Taylor, Philip E., et al. "Birch pollen rupture and the release of aerosols of respirable allergens." *Clinical & Experimental Allergy* 34.10 (2004): 1591-1596.

Technical Specifications OPC-N3 Particle Monitor. (2019). Alphasense Ltd. https://www.alphasense.com/wp-content/uploads/2022/09/Alphasense_OPC-N3_datasheet.pdf.

Todt, Michael A., et al. "Baseline Balloon Stratospheric Aerosol Profiles (B2SAP)—Systematic measurements of aerosol number density and size." *Journal of Geophysical Research: Atmospheres* 128.12 (2023): e2022JD038041.

Visez, Nicolas, et al. "Wind-induced mechanical rupture of birch pollen: Potential implications for allergen dispersal." *Journal of Aerosol Science* 89 (2015): 77-84.

Yu, Xiawei, et al. "Ambient measurement of fluorescent aerosol particles with a WIBS in the Yangtze River Delta of China: potential impacts of combustion-related aerosol particles." *Atmospheric Chemistry and Physics* 16.17 (2016): 11337-11348.

Yue, Siyao, et al. "Biological and nonbiological sources of fluorescent aerosol particles in the urban atmosphere." *Environmental Science & Technology* 56.12 (2022): 7588-7597.

Zhang, Yingxiao, et al. "Effects of pollen on hydrometeors and precipitation in a convective system." *Journal of Geophysical Research: Atmospheres* 129.6 (2024): e2023JD039891.

APPENDIX: SUPPLEMENTAL FIGURES

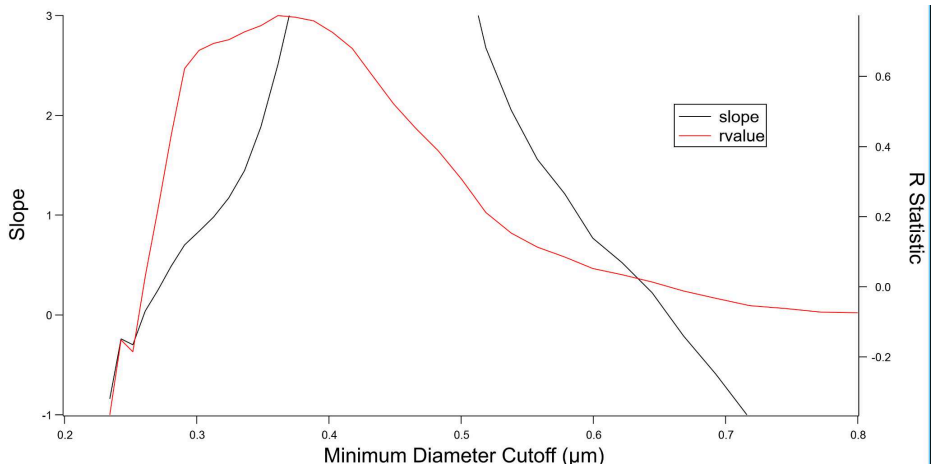

Figure 1S: results of correlation test between merged size distribution and colocated OPC data for submicron particles from 6/10/2023-6/12/2023, as described in section 2.5

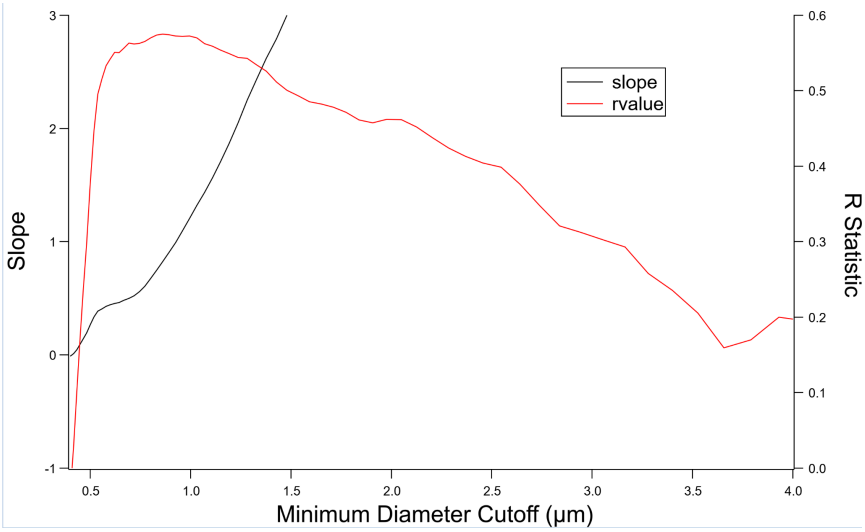

Figure 2S: same as figure 1S, for supermicron channel.

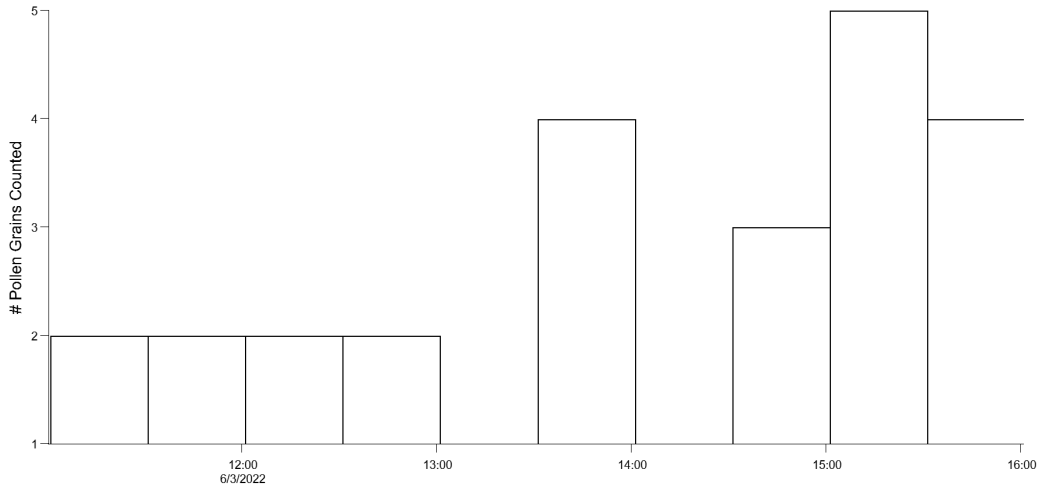

Figure 3S: Pollen grains counted on the spore trap during the 6/3/2022 case study. Data courtesy of Betsy Stone, University of Iowa.

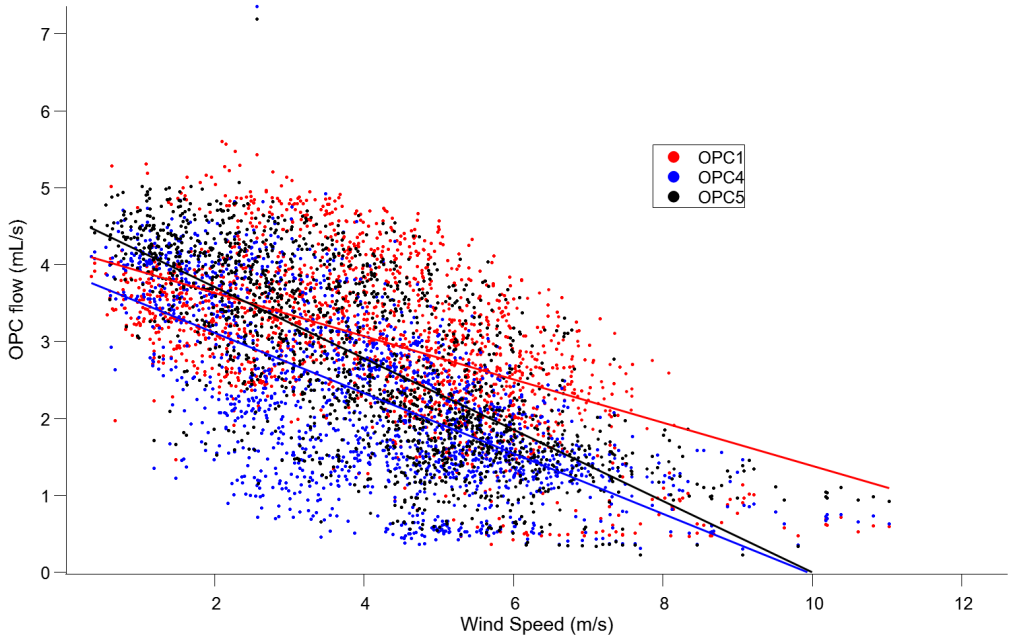

Figure 4S: relationship between surface wind speed and OPC measured flow rate for drone-mounted OPCs during selected grounded periods.